Title

CTLA4 depletes T cell endogenous and trogocytosed B7 ligands via cis-endocytosis.

Journal

Journal of Experimental Medicine, 220(7)

Authors

Xu, Xiaozheng

Dennett, Preston

Zhang, Jibin

et al.

Publication Date

2023-07-03

DOI

10.1084/jem.20221391

JEM Journal of Experimental Medicine

ARTICLE

CTLA4 depletes T cell endogenous and trogocytosed B7 ligands via cis-endocytosis

Xiaozheng Xu[1,2*], Preston Dennett[1,3*], Jibin Zhang[1*], Alice Sherrard[4], Yunlong Zhao[1], Takeya Masubuchi[1], Jack D. Bui[5], Xu Chen[2], and Enfu Hui[1]

CD28 and CTLA4 are T cell coreceptors that competitively engage B7 ligands CD80 and CD86 to control adaptive immune responses. While the role of CTLA4 in restraining CD28 costimulatory signaling is well-established, the mechanism has remained unclear. Here, we report that human T cells acquire antigen-presenting-cell (APC)–derived B7 ligands and major histocompatibility complex (MHC) via trogocytosis through CD28:B7 binding. Acquired MHC and B7 enabled T cells to autostimulate, and this process was limited cell-intrinsically by CTLA4, which depletes B7 ligands trogocytosed or endogenously expressed by T cells through cis-endocytosis. Extending this model to the previously proposed extrinsic function of CTLA4 in human regulatory T cells (Treg), we show that blockade of either CD28 or CTLA4 attenuates Treg-mediated depletion of APC B7, indicating that trogocytosis and CTLA4-mediated cis-endocytosis work together to deplete B7 from APCs. Our study establishes CTLA4 as a cell-intrinsic molecular sink that limits B7 availability on the surface of T cells, with implications for CTLA4-targeted therapy.

Introduction

CTLA4 is an essential coinhibitory receptor induced by T cell activation to maintain immune homeostasis (Schildberg et al., 2016). CTLA4 hypofunction results in autoimmunity, while its high expression is associated with immunosuppression and restricted T cell function in cancer and chronic viral infection (Attanasio and Wherry, 2016; Kuehn et al., 2014; Wing et al., 2008). On this basis, anti-CTLA4 therapeutic antibodies have been developed to block CTLA4 binding with the B7 costimulatory ligands CD80 and CD86 (referred to collectively as CD80/86 or "B7"). This method of CTLA4-targeted immunotherapy can restore antitumor immunity, producing durable elimination of disease in varying subsets of patients with certain cancers (Leach et al., 1996; Ribas and Wolchok, 2018). However, the precise mechanism of CTLA4 function has remained ambiguous and controversial (Schildberg et al., 2016; Walker and Sansom, 2015).

Under the current paradigm, CTLA4 prevents the T cell costimulatory receptor CD28 from engaging B7 ligands on professional APCs (Schildberg et al., 2016; Wei et al., 2018). The role of CTLA4 in restraining CD28 signaling has been demonstrated genetically by the rescue of the lethal autoimmune phenotype of CTLA4-deficient mice upon codeletion of CD28 or both B7 ligands (Salomon and Bluestone, 2001; Tai et al., 2007). Additionally, CTLA4 ectodomain fused with an immunoglobulin domain (CTLA4-Ig), which blocks CD28:B7 interactions, has been effective in treating certain autoimmune disorders (Kremer et al., 2003; Wertheimer et al., 2021). While these results demonstrate that key elements of CTLA4 regulation can be recapitulated via blockade of B7 alone, the endogenous inhibitory function of CTLA4 appears more complex and dependent on its highly conserved intracellular domain (Teft et al., 2006), which promotes constitutive endocytosis resulting in a predominately intracellular vesicular localization of CTLA4 (Leung et al., 1995).

In response to TCR stimulation, CTLA4 becomes polarized to the cell surface, where it reportedly exerts both cell-intrinsic and -extrinsic inhibitory effects to regulate adaptive immune responses (Egen and Allison, 2002; Walker and Sansom, 2015; Wing et al., 2011). Unlike typical inhibitory immunoreceptors, CTLA4 does not appear to recruit intracellular phosphatases and is thought to function primarily via CD28 signal deprivation (Walker and Sansom, 2015). These findings have contributed to

[1]Department of Cell & Developmental Biology, University of California, San Diego, La Jolla, CA, USA; [2]Department of Neurosciences, University of California, San Diego, La Jolla, CA, USA; [3]Department of Chemistry and Biochemistry, University of California, San Diego, La Jolla, CA, USA; [4]Department of Genetics, Yale University School of Medicine, New Haven, CT, USA; [5]Department of Pathology, University of California, San Diego, La Jolla, CA, USA.

*X. Xu, P. Dennett, and J. Zhang contributed equally to this paper. Correspondence to Enfu Hui: enfuhui@ucsd.edu; Preston Dennett: prestondennett@gmail.com

X. Xu's current affiliation is Sanofi Institute for Biomedical Research, Jiangsu, China.

a model of cell-intrinsic inhibition by CTLA4 termed "negative costimulation," which is thought to occur via direct competition with CD28 at the cell surface during T cell priming (Wei et al., 2019). While this notion is consistent with the numerous seemingly cell-intrinsic effects of CTLA4 expression, including fine control of T cell clonal expansion and differentiation, it does not fully account for features of CTLA4 that appear optimized for B7 ligand depletion (Greenwald et al., 2001; Metz et al., 1998; Schneider et al., 2006; Tai et al., 2012; Walker and Sansom, 2015). Moreover, current cell-intrinsic models of CTLA4 function have been opposed by the observation that the presence of high CTLA4-expressing T cells is sufficient to prevent lethal autoimmune pathology of CTLA4-deficient cells in trans in reconstituted bone marrow chimera mice (Bachmann et al., 1999). This finding has supported a primarily cell-extrinsic model of CTLA4 function (Walker and Sansom, 2011) termed the "trans-endocytosis" model, which postulates that CTLA4 directly internalizes B7 displayed by APCs in trans and mediates its degradation to inhibit subsequent T cell:APC signaling interactions (Qureshi et al., 2011).

Despite evidence that T cell expression of high levels of CTLA4 results in internalization and degradation of exogenous B7 ligands, the trans-endocytosis model and a purely cell-extrinsic mechanism of CTLA4 function has been unable to account for cell-intrinsic effects of CTLA4. One notable limitation is the difficulty to extend an extrinsic framework to conventional $CD4^+$ (Tconv) and $CD8^+$ T cells where CTLA4 surface expression is very low.

It is increasingly appreciated that during activation, T cells acquire APC-derived surface molecules via trogocytosis, a contact-dependent cellular ingestion process conserved in eukaryotes (Davis, 2007; Nakada-Tsukui and Nozaki, 2021). As a consequence of trogocytosis, T cells redisplay APC-derived ligands on their surface and can thereby act as APCs to stimulate other T cells. Such T–T interactions have been implicated in collective regulation of T cell proliferation and differentiation during the initiation and propagation of immune responses (Gérard et al., 2013; Helft et al., 2008; Zenke et al., 2020; Zenke et al., 2022). Along this line, CD28:B7 interactions reportedly induce trogocytosis of B7 ligands alongside various "bystander" surface molecules from APCs, including peptide antigen (MHC; Hwang et al., 2000; Sabzevari et al., 2001; Tatari-Calderone et al., 2002; Watanabe et al., 2022). More recently, using an endocytosis-deficient CTLA4 mutant, Sakaguchi and colleagues provided evidence that CTLA4 also mediates trogocytosis of B7 ligands and lipid molecules from APCs rather than trans-endocytosis (Tekguc et al., 2021). However, the functional implications of trogocytosis vs. trans-endocytosis of B7 ligands by CTLA4 and how it intercepts with CD28 to regulate the effects of this process during subsequent T–T communications is unclear.

Indeed, trogocytosis and trans-endocytosis are occasionally conflated in the literature, but they differ both mechanistically and functionally. Trans-endocytosis refers to specific and direct internalization of receptor/ligand complexes resulting in their removal from the target cell without redisplay on recipient cells (Parks et al., 2000). In contrast, trogocytosis refers to contact-dependent acquisition of plasma membrane fragments that results in functional redisplay of exogenous surface molecules on recipient cells (Joly and Hudrisier, 2003). Despite being promoted by specific receptor/ligand interactions, trogocytosis is invariably associated with nonspecific cotransfer of bystander surface molecules, which are similarly redisplayed alongside specifically acquired ligands (Miyake and Karasuyama, 2021). In light of the increasingly appreciated physiological significance of trogocytosis and its ability to facilitate T–T antigen presentation (Akkaya et al., 2019; Boccasavia et al., 2021; Schriek et al., 2022), we tested the hypothesis that CTLA4 can act in cis to deplete B7 molecules displayed by T cells alongside acquired peptide antigens (pMHC). Our experiments revealed a T cell–intrinsic mechanism of CTLA4 function that incorporates its highly endocytic feature and accounts for its cell-extrinsic regulatory effects, with implications for clarifying the mechanistic basis of its control of immune homeostasis.

Results

CD28 mediates T cell acquisition of APC-derived, CD80-containing membrane fragments

Upon contact with APCs, T cells rapidly acquire and redisplay APC-derived plasma membrane fragments and associated surface molecules via trogocytosis (Joly and Hudrisier, 2003). In light of conflicting reports over the mechanism of B7 transfer through trogocytosis (Tekguc et al., 2021) or trans-endocytosis (Qureshi et al., 2011), we examined B7 acquisition from APCs by T cells in the context of CTLA4-expression using light and electron microscopy (EM). We generated Jurkat T cell lines expressing CTLA4-mCherry and *CD80*$^{-/-}$*CD86*$^{-/-}$ Raji B cells expressing CD80-GFP, and after 1 h coculture, we observed extensive CD80-GFP transfer from Raji to Jurkat cells. While some GFP signal acquired by Jurkat cells colocalized with CTLA4 in intracellular vesicles (Fig. 1 A, left), as reported (Qureshi et al., 2011), we also noted that substantial CD80-GFP acquired by Jurkat did not colocalize with CTLA4, particularly for puncta displayed at the cell surface (Fig. 1 A, left, white arrowhead). Moreover, using correlative light electron microscopy, we observed discrete Raji-derived membrane fragments associated with the Jurkat surface (Fig. 1 A, right, red arrowhead). These imaging data suggest that T cells can acquire CD80-containing membrane fragments from APCs and that acquired CD80 accumulates in $CTLA4^+$ vesicles.

The absence of CTLA4 in $CD80\text{-}GFP^+$ puncta at the Jurkat cell surface implies a CTLA4-independent mechanism of B7 transfer. Since T cells constitutively express CD28, which reportedly mediates B7 trogocytosis by T cells (Sabzevari et al., 2001), we next investigated the relative contribution of CD28 and CTLA4 in mediating B7 intercellular transfer. To this end, we engineered *CD28*$^{-/-}$*CD28-mCherry*$^+$*CTLA4-HaloTag*$^+$ Jurkat T cells, briefly cocultured these cells with *CD80*$^{-/-}$*CD86*$^{-/-}$*CD80-GFP*$^+$ Raji B cells for 15 min, and visualized CD28, CTLA4, and CD80 simultaneously at the T-cell:APC interface. Confocal microscopy revealed that Raji cells extended $CD80^+$ membrane projections across the Jurkat surface and that these membrane structures appeared to become bound by CD28 while showing minimal colocalization with CTLA4 (Fig. 1 B), which displayed a characteristic

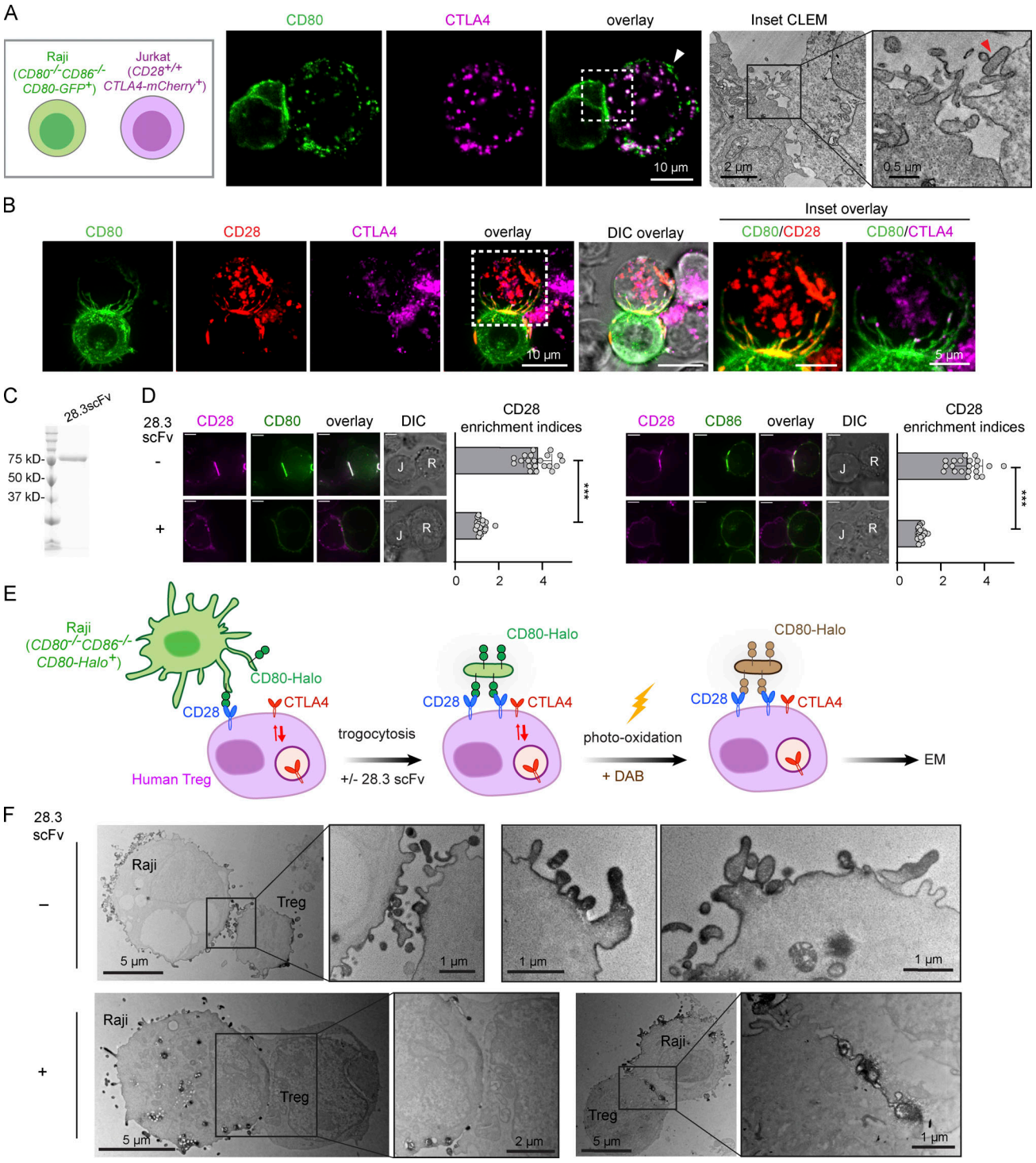

Figure 1. **CD28 mediates acquisition of APC-derived membrane fragments upon B7 binding. (A)** Left: Confocal microscopy of a conjugate between a CD80-GFP$^+$ Raji B cell and a CD80-GFP$^+$ Jurkat T cell. Image shows CD80-GFP accumulation in CTLA4-associated vesicles and CTLA4-independent acquisition of membrane fragments enriched in CD80-GFP (white arrowhead). Right: Correlated light electron micrograph (CLEM) of confocal inset in A. Red arrowhead indicates discrete membrane fragments acquired by Jurkat from Raji APC. **(B)** Confocal micrographs of *CD28*$^{-/-}$ Jurkat cells co-expressing CD28-mCherry and CTLA4-HaloTag (JFX-646) in conjugation with *CD80*$^{-/-}$*CD86*$^{-/-}$ Raji cells expressing CD80-GFP. Insets show CD28 and CTLA4 colocalization with Raji-derived membrane projections. **(C)** Coomassie brilliant blue stained SDS-PAGE of purified MBP-28.3scFv. **(D)** Representative confocal micrographs of a Raji (*CD80*$^{-/-}$*CD86*$^{-/-}$*CD80-GFP*$^+$):Jurkat (*CD28*$^{-/-}$*CD28-mCherry*$^+$) conjugate (left) and a Raji (*CD80*$^{-/-}$*CD86*$^{-/-}$*CD86-GFP*$^+$):Jurkat (*CD28*$^{-/-}$*CD28-mCherry*$^+$) conjugate (right), with or without the presence of 28.3scFv. Scatter plots on the immediate right show the synaptic enrichment indices of CD28. In differential interference contrast (DIC) images, R denotes Raji, J denotes Jurkat. Scale bar: 5 µm. *n* = 20 conjugates. **(E)** Cartoon depicting EM labeling strategy of human regulatory T cells following conjugation with Raji B cells expressing CD80-HaloTag (JFX-549). Laser excitation at 561 nm induces oxidative polymerization of electron-dense DAB proximal to CD80. **(F)** Representative electron micrographs of human Treg cells upon contact with Raji APC expressing CD80-Halo in the

presence or absence of 28.3scFv, with CD80-Halo stained by DAB. The rightmost two images under the −28.3scFv condition show zoomed in view of another Treg cell after Raji contact, highlighting possible fusion of CD80-Halo–associated membrane fragments. Error bars in D are SD from 20 Raji:Jurkat conjugates under each indicated condition. ***, P < 0.001; Student's *t* test. Source data are available for this figure: SourceData F1.

primarily intracellular localization. This result suggests that CD28, and to a lesser extent CTLA4, mediate the capture of APC-derived, CD80-containing membrane fragments during initial cell–cell contacts.

We next determined whether the blockade of CD28:B7 interactions inhibits membrane transfer from Raji APCs using EM. To block B7 without activating CD28 due to crosslinking, we produced recombinant single-chain variable fragment (scFv) of a B7-blocking anti-CD28 antibody CD28.3 (Vanhove et al., 2003), abbreviated as 28.3scFv hereafter (Fig. 1 C). As a proof-of-principle, when we conjugated *CD28*$^{-/-}$*CD28-mCherry*$^{+}$ Jurkat T cells with *CD80*$^{-/-}$*CD86*$^{-/-}$*CD80-GFP*$^{+}$ or *CD80*$^{-/-}$*CD86*$^{-/-}$*CD86-GFP*$^{+}$ Raji APCs, 28.3scFv treatment prevented the coenrichment of CD28 and CD80/CD86 to the Jurkat:Raji interface (Fig. 1 D). Having established this CD28 blocking agent, we purified human Tregs (CD4^{+}CD25^{high}CD127^{low}) from peripheral blood mononuclear cells (PBMCs) and incubated these cells with Raji B cells expressing CD80-HaloTag to enable visualization of membrane transfer by EM. Following a 15-min coculture, we fixed the cells and labeled CD80-HaloTag with an electron-dense polymer of 3′3′-diaminobenzidine (DAB) via photo-oxidation of JFX549 Halo ligand (Fig. 1 E; Maranto, 1982). EM micrographs revealed association of Tregs with APC-derived membrane fragments indicated by DAB staining. Interestingly, some DAB-stained membrane components appeared to have fused with the Treg cell membrane (Fig. 1 F, −28.3scFv condition). Strikingly, in the presence of 28.3scFv, membrane transfer appeared to be largely eliminated despite high CTLA4 expression (Fig. 1 F, +28.3scFv condition).

Collectively, these data suggest that during T cell:APC contacts, CD28 induces direct capture and incorporation of APC-derived membrane fragments upon CD80 binding, while a subset of acquired CD80 molecules accumulate in CTLA4^{+} vesicles.

CD28 and to a lesser extent CTLA4 expressed by human T cells mediate rapid B7 trogocytosis upon contact with APCs

We next sought to more quantitatively examine the roles of CD28 and CTLA4 in mediating trogocytosis of B7 molecules by human primary T cells during coculture with Raji B cells. We purified human Treg and Tconv from PBMCs of three independent age-matched donors per experiment. Freshly purified human Tregs expressed high CD25, low CD127, and FoxP3, whereas human Tconvs expressed low CD25, high CD127, and little FoxP3. Moreover, both Treg and Tconv cells expressed both CD28 and CTLA4 while Tregs remained FoxP3 positive during culture with anti-CD3/anti-CD28 stimulation (Fig. 2 A).

Considering that trogocytosis occurs rapidly during cell–cell contact (Joly and Hudrisier, 2003), we sought to set up a brief coculture system to induce contact-dependent B7 transfer from Raji APCs to T cells. In this assay, we asked how blockade of CD28:B7 interaction via 28.3scFv (Fig. 1, C and D) or blockade of CTLA4:B7 interaction via ipilimumab (He et al., 2017) affects B7 transfer from Raji APCs to T cells.

We first examined the roles of CD28 or CTLA4 in mediating CD80/CD86 acquisition by human Treg cells. We incubated human Tregs with *CD80*$^{-/-}$*CD86*$^{-/-}$*CD80-GFP*$^{+}$ or *CD80*$^{-/-}$*CD86*$^{-/-}$*CD86-GFP*$^{+}$ Raji cells, in the presence or absence of superantigen Staphylococcal Enterotoxin B (SEB), and the blocking agents ipilimumab and/or 28.3scFv. After 15 min coculture, we quantified CD80/CD86-GFP signal on Tregs by flow cytometry (Fig. 2 B, cartoon; see Fig. S1 A for gating strategy). In the presence of SEB and absence of any blocking agents, Tregs acquired considerable amounts of CD80-GFP or CD86-GFP (Fig. 2 B, "+, +, −, −"). Strikingly, CD28 blockade (Fig. 2 B, "+, +, −, +"), but not CTLA4 blockade (Fig. 2 B, "+, +, +, −"), markedly decreased B7 acquisition, and coblockade of CTLA4 and CD28 did not further inhibit B7 transfer (Fig. 2 B, "+, +, +, +"), supporting the notion that both CTLA4-mediated trogocytosis and/or trans-endocytosis were negligible under these conditions. A similar trend was seen in the absence of SEB (Fig. 2 B, −SEB conditions), despite less B7 acquisition than the corresponding SEB+ conditions, consistent with previous findings that CD28-dependent trogocytosis is enhanced by but does not require TCR stimulation (Tatari-Calderone et al., 2002).

We next examined B7 acquisition by human Tconvs (Fig. 2 C) and observed a similar pattern as for Tregs: antibody blockade of CD28 but not CTLA4 diminished the ability of Tconvs to trogocytose B7 molecules from APCs. These data suggest that rapid B7 acquisition by T cells is primarily mediated by CD28 rather than CTLA4 binding during initial contact with APCs.

CD28:B7 interactions induce trogocytosis of both B7 and MHC molecules in a largely TCR-independent manner

We further examined whether CD28 was necessary for rapid B7 acquisition using Jurkat lines, which endogenously express CD28 but not CTLA4 (Fig. S1 B). Notably, unlike human primary T cells, which endogenously express MHCII (HLA-DR) upon activation (Holling et al., 2004), Jurkat cells lack HLA-DR expression (Fig. S1 C). This feature allowed us to determine whether CD28-driven B7 acquisition is associated with bystander transfer of APC-derived MHCII to T cells.

After 15 min incubation with *CD80*$^{-/-}$*CD86*$^{-/-}$*CD80-GFP*$^{+}$ or *CD80*$^{-/-}$*CD86*$^{-/-}$*CD86-GFP*$^{+}$ Raji APCs in the presence of TCR stimulation by superantigen Staphylococcal Enterotoxin E (SEE), WT Jurkat cells acquired APC-derived CD80/CD86-GFP and HLA-DR (Fig. 2 D, "*CD28*$^{+/+}$, +, +" vs. "*CD28*$^{+/+}$, −, −"). Deletion of CD28 by CRISPR/Cas9 editing (Fig. S1 D) abolished CD80 and CD86 trogocytosis and markedly decreased HLA-DR transfer (Fig. 2 D, "*CD28*$^{-/-}$, +, +"), suggesting that in CTLA4-negative T cells, CD28 expression was both necessary and sufficient to induce B7/MHC acquisition upon APC contact. Notably, even in the absence of TCR stimulation, WT Jurkat cells acquired CD80/CD86 and HLA-DR via trogocytosis upon contact with Raji APCs

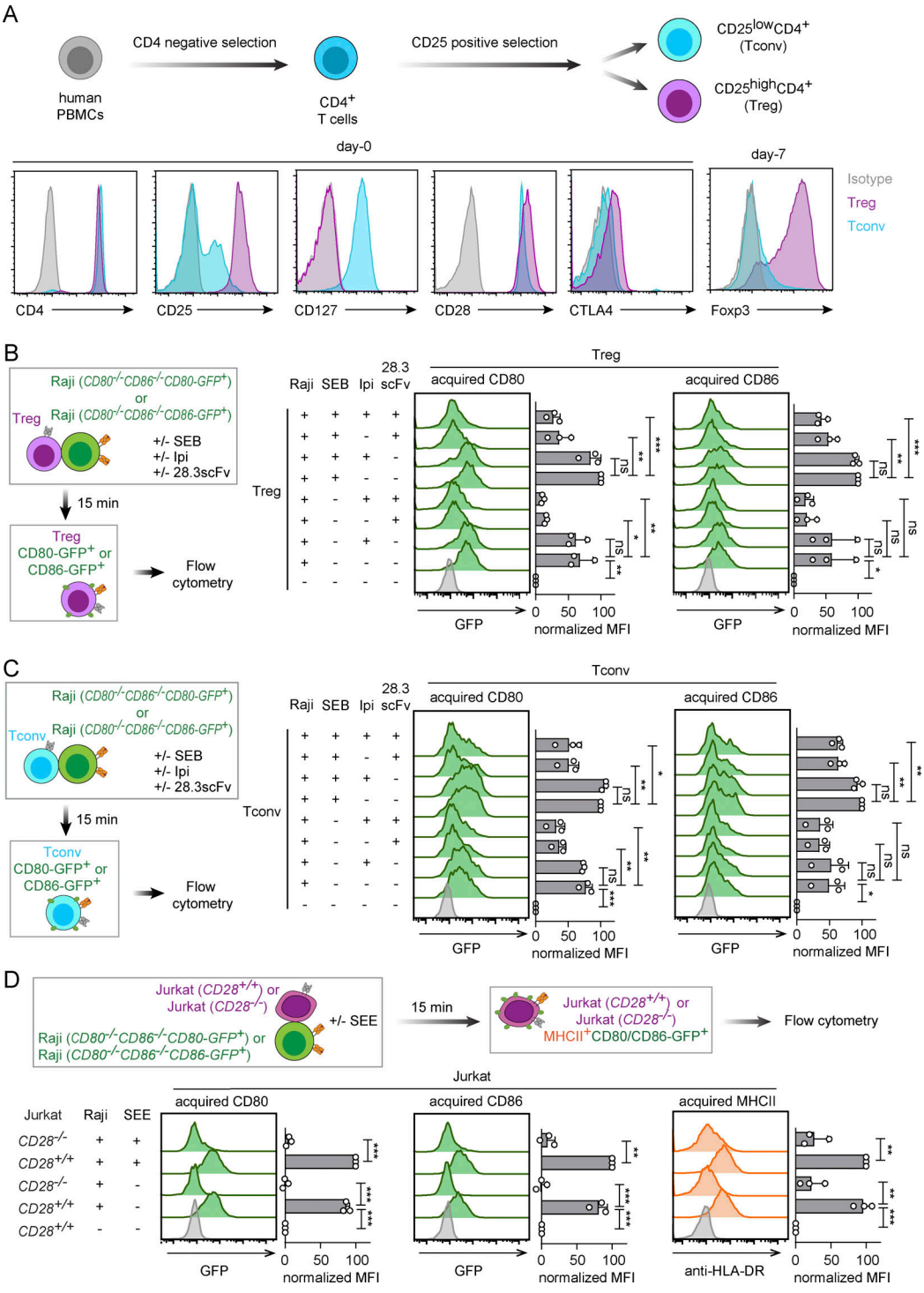

Figure 2. **CD28 expressed by human T cells mediate rapid B7 acquisition upon ligand binding. (A)** Scheme of Treg and Tconv isolation from human PBMCs. Flow cytometry histograms show surface expressions of CD4, CD25, and CD127 and intracellular expression of Foxp3 of purified Treg and Tconv cells. **(B)** Effects of CD28 blockade and CTLA4 blockade on the abilities of human Tregs to acquire CD80 and CD86 from Raji APCs. Left: A cartoon depicting a Treg: Raji (*CD80*$^{-/-}$*CD86*$^{-/-}$*CD80-GFP*$^{+}$) or Treg:Raji (*CD80*$^{-/-}$*CD86*$^{-/-}$*CD86-GFP*$^{+}$) coculture assay, after which GFP signal in Tregs was measured. Right: Representative flow cytometry histograms showing the amounts of CD80-GFP or CD86-GFP on Tregs after a 15-min incubation with Raji under the indicated conditions. Bar graphs on the immediate right show the normalized MFI values of acquired GFP on Tregs, calculated by setting the MFI of the "–, –, –, –" condition as 0 and the MFI of "+, +, –, –" condition as 100. **(C)** Same as in B except replacing human Tregs with Tconvs. **(D)** Effects of CD28 deficiency or blockade on the abilities of Jurkat to acquire CD80, CD86, and MHCII. Upper: A cartoon depicting the assay setup. Lower: Representative flow cytometry histograms showing the relative levels of acquired CD80, CD86, or MHCII on the indicated Jurkat cells after a 15-min incubation with either Raji (*CD80*$^{-/-}$*CD86*$^{-/-}$*CD80-GFP*$^{+}$) or Raji (*CD80*$^{-/-}$*CD86*$^{-/-}$*CD86-GFP*$^{+}$) cells. Bar graphs immediate right show the normalized MFI values of acquired CD80-GFP, CD86-GFP, or HLA-DR on Jurkat cells, calculated by setting the MFI of "–, –, –" condition as 0 and the MFI of "+, +, –" condition as 100. Error bars are SD from three independent coculture experiments performed on three different days, data in B and C were generated using PBMCs from three independent age-matched donors. *, P < 0.05; **, P < 0.01; ***, P < 0.001; unpaired two-tailed Student's *t* test.

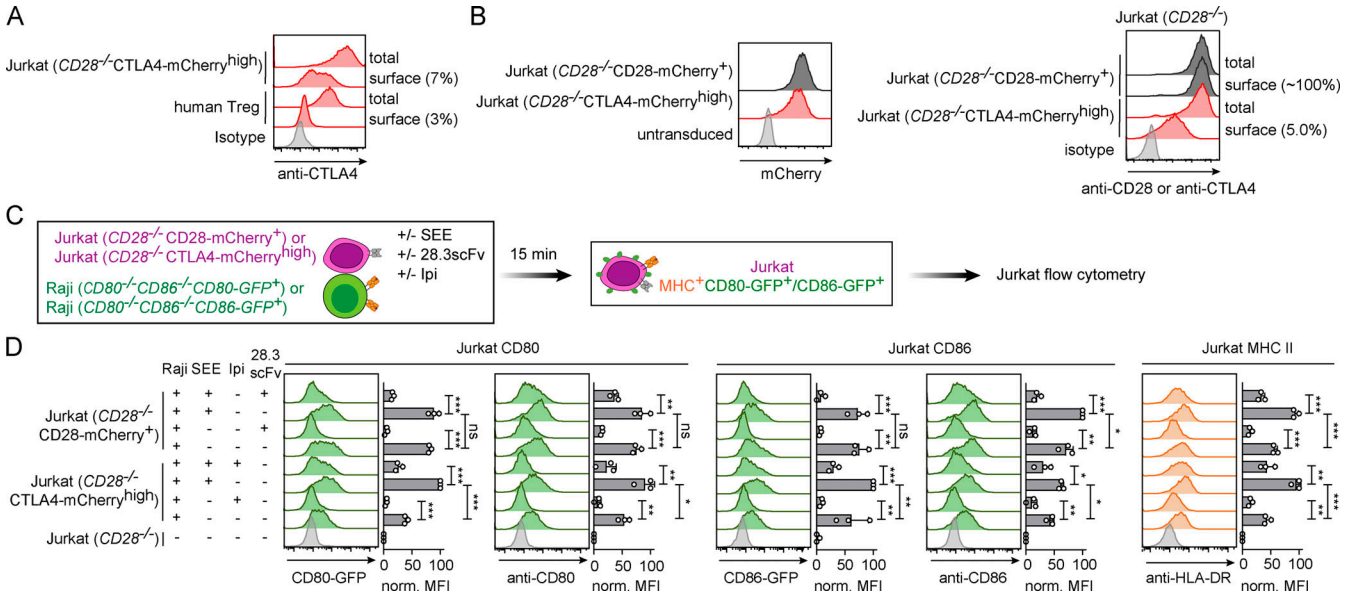

Figure 3. **CTLA4-mediated trogocytosis is promoted by TCR stimulation. (A and B)** Flow cytometry histograms showing total and surface levels of CD28 and CTLA4 on indicated Jurkat cells. Total and surface staining was conducted with permeabilized and unpermeabilized cells, respectively. Numbers in parentheses indicate percentages of surface CD28 or CTLA4. **(C)** Schematics of a Jurkat:Raji coculture assay examining CD28 or CTLA4-mediated trogocytosis (acquisition) of B7 and MHC from APCs. **(D)** Effects of CTLA4 or CD28 blockade on the abilities of indicated Jurkat to acquire CD80, CD86, or MHCII. Representative flow cytometry histograms and MFI values showing the CD80-GFP (reflecting total CD80), anti-CD80 (reflecting surface CD80), CD86-GFP (reflecting total CD86), anti-CD86 (reflecting surface CD86), or anti–HLA-DR (reflecting surface MHCII) in indicated Jurkat after a 15-min incubation with Raji (*CD80*$^{-/-}$*CD86*$^{-/-}$*CD80-GFP*$^{+}$) or Raji (*CD80*$^{-/-}$*CD86*$^{-/-}$*CD86-GFP*$^{+}$) cells under the indicated conditions. Bar graphs immediate right show the normalized MFI (norm MFI) values of acquired CD80-GFP, anti-CD80, CD86-GFP, anti-CD86, or anti–HLA-DR on Jurkat cells, calculated by setting the MFI of "*CD28*$^{-/-}$ Jurkat –, –, –, –" condition as 0 and the condition with the highest MFI value as 100 in each replicate. Error bars are SD from three independent coculture experiments performed on three different days. *, P < 0.05; **, P < 0.01; ***, P < 0.001; unpaired two-tailed Student's *t* test.

(Fig. 2 D, "*CD28*$^{+/+}$, +, –" vs. "*CD28*$^{+/+}$, –, –"). Thus, CD28:B7 interactions can mediate trogocytosis of both B7 and MHCII by T cells in a largely TCR-independent manner.

CTLA4:B7 interactions induce trogocytosis of B7 ligands and MHC in a TCR-promoted manner

We next tested the ability of CTLA4 to mediate trogocytosis in the absence of CD28 and transduced CD28-deficient Jurkat cells to express CTLA4-mCherry at a high level, ∼8-fold higher than CTLA4 surface expression in human Tregs (Fig. 3 A). Anti-CTLA4 staining of permeabilized and intact cells showed that CTLA4-mCherry was largely intracellular, with ∼7% surface localization (Fig. 3 A), consistent with the highly endocytic feature of CTLA4 (Leung et al., 1995). Parallel staining of human Tregs showed 3% surface localization of CTLA4 (Fig. 3 A). As controls, we also transduced CD28-deficient Jurkat cells to express CD28-mCherry, at a level similar to CTLA4-mCherry in CTLA4 high Jurkat, indicated by both mCherry signal and antibody staining (Fig. 3 B). As expected, anti-CD28 staining of permeabilized and intact cells revealed nearly 100% surface localization of CD28.

We incubated each of the aforementioned Jurkat T cell lines with Raji APCs for 15 min and examined CD80, CD86, and HLA-DR levels on the Jurkat (Fig. 3 C). CD28-deficient Jurkat cells expressing high CTLA4-mCherry acquired both CD80/CD86-GFP and HLA-DR in a manner that was inhibited by ipilimumab treatment (Fig. 3 D, *CD28*$^{-/-}$*CTLA4-mCherry*^{high}), demonstrating that CTLA4:B7 interactions can induce B7 and bystander MHC acquisition via trogocytosis. In parallel experiments, we observed similar B7/MHC acquisition by CD28-deficient Jurkat expressing CD28-mCherry in a 28.3scFv-sensitive fashion as expected (Fig. 3 D, *CD28*$^{-/-}$*CD28-mCherry*$^{+}$). Notably, akin to CD28-driven ligand acquisition, the CTLA4-driven process was associated with redisplay of both acquired B7 as well as MHC molecules, as evidenced by antibody surface staining (Fig. 3 D, anti-CD80, anti-CD86, and anti-HLA-DR). This bystander transfer and redisplay are hallmarks of trogocytosis rather than trans-endocytosis, which has been defined by direct internalization of ligand:receptor complexes without redisplay (Parks et al., 2000; Qureshi et al., 2011).

TCR stimulation appeared to more strongly promote CTLA4-mediated trogocytosis than CD28-mediated trogocytosis (Fig. 3 D, +SEE conditions), consistent with TCR-dependent delivery of CTLA4 to cell surface (Egen and Allison, 2002). Moreover, the presence of SEE induced appreciable transfer of MHC molecules even under the CD28 or CTLA4 blockade condition, evidence of TCR-mediated trogocytosis of MHC, as reported (Patel et al., 2001). Thus, these results suggested that exogenous MHC can be transferred to T cells through both a TCR-dependent mode and a bystander mode driven by either CD28 or CTLA4 interactions with B7 ligands. These results demonstrate that either CD28 or CTLA4 can independently mediate trogocytosis of B7 and MHC, leading to redisplay of these ligands on the surface of T cells.

Given that both CD28 and CTLA4 can mediate trogocytosis of B7/MHC, we next investigated why B7 trogocytosis by human primary T cells was more sensitive to CD28 blockade than CTLA4 blockade, as observed in Fig. 2. We noted that CTLA4 expression on human Tregs was much lower than that in the CTLA4^{High} Jurkat (see Fig. 3 A for comparison of both total and surface CTLA4 levels). Hence, we speculated that the relatively low level of CTLA4 in human primary T cells likely limits its contribution to B7/MHC trogocytosis. Supportive of this notion, when we cultured Raji cells with engineered Jurkat (*CD28*$^{+/+}$CTLA4^{high}) cells, which expressed similar levels of CD28 (~2-fold higher) and ~20-fold higher CTLA4 than did human Tregs (Fig. S2 A), CTLA4 blockade suppressed B7 acquisition, with a magnitude that was comparable with CD28 blockade (Fig. S2 B). As expected, the presence of SEE potentiated B7 acquisition and increased the relative contribution of CTLA4 (Fig. S2 B).

Altogether, the quantitative measurements with engineered Jurkat lines demonstrate that both CD28 and CTLA4 are capable of mediating B7/MHC trogocytosis upon B7 binding, leading to redisplay of these ligands on T cell surface. However, in primary human Treg and Tconv cells, CD28 was observed to outcompete CTLA4 in driving B7/MHC acquisition via trogocytosis during initial contacts, likely due to the low surface expression of CTLA4.

Acquired MHCII and B7 enable human T cells to autostimulate, a process restricted by CTLA4:B7 interactions

We next investigated whether trogocytosed B7 ligands can support T cell priming in the presence of B7 high professional APCs. We preconditioned CD4$^+$ T cells with *CD80*$^{-/-}$*CD86*$^{-/-}$*CD80-GFP*$^+$ Raji cells in the absence of antigen to allow for acquisition of CD80-GFP and MHC or with *CD80*$^{-/-}$*CD86*$^{-/-}$ Raji as a control and purified the T cells using FACS (Fig. S3 A). Upon coculture with human monocyte-derived mature dendritic cells (DCs; CD14$^-$CD209$^+$CD83$^+$HLA$^+$CD40$^+$CD80$^+$CD86$^+$; Fig. S3 B), T cells preconditioned with *CD80*$^{-/-}$*CD86*$^{-/-}$*CD80-GFP*$^+$ Raji produced more IL2 and IFNγ than those preconditioned with *CD80*$^{-/-}$*CD86*$^{-/-}$ Raji, especially at a lower DC to T ratio and earlier time points (Fig. 4 A), consistent with the notion that trogocytosed CD80 can promote T cell priming.

Prior studies have shown that trogocytosed B7 and MHC endow T cells with the capacity to act as APCs by stimulating other T cells through both CD28 and TCR axes (Sabzevari et al., 2001; Xiang et al., 2005; Zenke et al., 2022). Given the current model that CTLA4 inhibits B7:CD28 interactions during T cell conjugation with professional APCs, we next examined whether CTLA4 could restrict T–T autostimulation in the absence of APCs. We first preconditioned human CD4$^+$ T cells with Raji APCs deficient in both B7 ligands (*CD80*$^{-/-}$*CD86*$^{-/-}$) or with Raji expressing CD80-GFP (*CD80*$^{-/-}$*CD86*$^{-/-}$*CD80-GFP*$^+$) in the absence of antigen to allow for CD80 trogocytosis without TCR stimulation. We then purified the resulting CD4$^+$ T cells by FACS to remove Raji APCs and incubated them with SEB in the presence or absence of ipilimumab to prevent CTLA4:B7 binding (Fig. 4 B). ELISA showed that T cells preconditioned by Raji (*CD80-GFP*$^+$) cells produced markedly more IL-2 than those preconditioned by Raji (*CD80*$^{-/-}$*CD86*$^{-/-}$) over a range of several days, indicating autostimulation of MHC/B7-dressed T cells. Importantly, this IL-2 production was significantly enhanced by ipilimumab treatment from day 2–4 (Fig. 4 B). These data suggested that CTLA4 can act directly on T cells to inhibit the activity of B7 captured by CD28-mediated trogocytosis in the absence of professional APCs.

CTLA4 acts in cis to deplete CD80 but not MHC in human Treg and Tconv cells in a TCR-promoted manner

Tregs are able to downregulate B7 molecules on professional APCs in a CTLA4 and cell–cell-contact-dependent manner (Wing et al., 2008). Our result that CTLA4:B7 interactions inhibit autostimulation of human CD4$^+$ T cells (Fig. 4 B) suggests that CTLA4 can directly control functional levels of B7 within a T cell population. In principle, this inhibition of CD28:B7 interactions on T cells by CTLA4 might occur either in a cell-extrinsic manner via trans-endocytosis between B7-displaying T cells or through a cell-intrinsic mechanism to deplete B7 molecules in cis from the same T cell surface. To determine if cis-endocytosis takes place, we followed the fate of CD80 on human T cells in the presence or absence of excess filler cells to inhibit trans contacts.

After preconditioning human Tregs with *CD80*$^{-/-}$*CD86*$^{-/-}$*CD80-GFP*$^+$ Raji APCs, we immediately purified *GFP*$^+$ Tregs by FACS and cultured these cells as a monolayer in the presence of 30-fold excess *CD28*$^{-/-}$ Jurkat "filler" cells to block T–T contacts and therefore CTLA4 trans-interactions (Fig. 5 A and Fig. S4). We noted that activated human Tregs expressed both CD80 and HLA-DR even prior to contact with Raji cells (Fig. 5 B, "Treg untreated"). However, preincubation with Raji cells increased both CD80 and HLA-DR on Tregs (Fig. 5 B, "0 h, –, –, –" vs. "Treg untreated"), consistent with CD28-induced trogocytosis. Notably, this elevated CD80 on Tregs decreased by 72.3% after 9 h incubation with filler cells, whereas elevated HLA-DR levels remained unaltered (Fig. 5 B, "0 h, –, –, -" vs. "9 h, +, –, –"). Thus, Tregs deplete CD80 but not HLA-DR from the cell surface in a cell-intrinsic fashion. Strikingly, blockade of CTLA4:CD80 interaction using ipilimumab preserved CD80 levels on Tregs, increasing CD80 at 9 h by 2.7-fold, from 27.7 to 74.7% of initial amounts following acquisition at 0 h (Fig. 5 B, "9 h, +, –, –" vs. "9 h, +, +, –"). In contrast, CD28 blockade only slightly increased in CD80 on Tregs after 9 h incubation (Fig. 5 B, "9 h, +, –, –" vs. "9 h, +, –, +"). CD80 level in the CTLA4/CD28 coblockade condition was similar to CTLA4 mono-blockade condition (Fig. 5 B, "9 h, +, +, +" vs. "9 h, +, +, –"). These data indicate that CTLA4 can act in cis to deplete CD80 from the Treg surface.

In the absence of filler cells, CD80 was lowered across all four conditions (Fig. 5 B, "w/o filler cells" conditions), but the effects of CTLA4 and CD28 blockade were notably similar as in the presence of excess filler cells: CTLA4 blockade again preserved CD80 levels on Tregs, increasing CD80 by threefold after 9 h incubation, from 20.1 to 59.8% of the initial amounts (Fig. 5 B, "9 h, –, –, –" vs. "9 h, –, +, –"); CD28 blockade again marginally increased remaining CD80 levels (Fig. 5 B, "9 h, –, –, –" vs. "9 h, –, –, +"). Thus, under these conditions, CTLA4-mediated depletion of B7 occurs largely in cis, with minimal acceleration of CTLA4-dependent B7 depletion observed in the presence of T–T

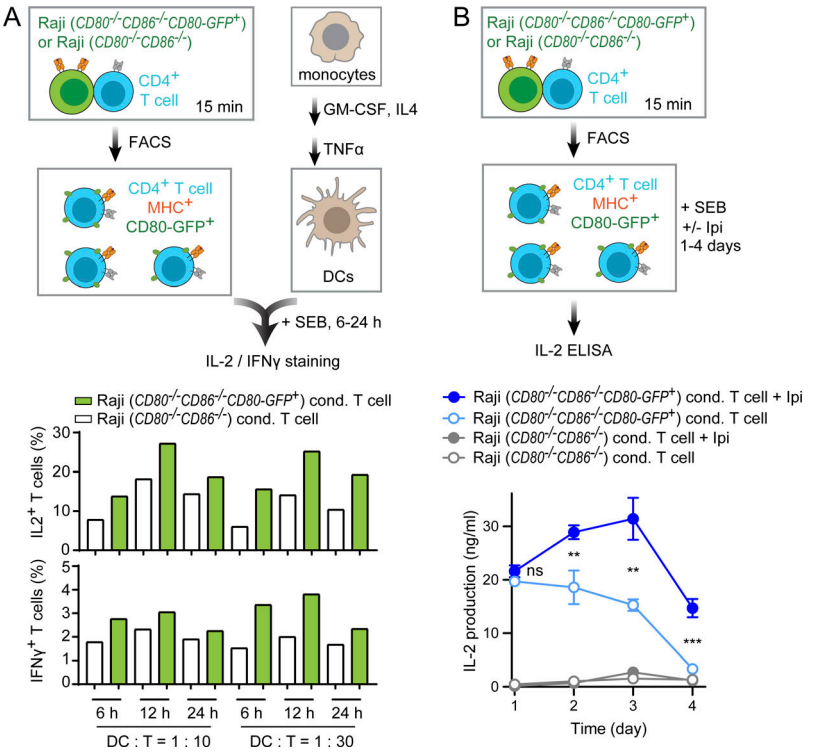

Figure 4. **CTLA4 restricts autostimulation of CD4⁺ T cells displaying APC-derived CD80. (A)** Human CD4⁺ T cells, purified from PBMCs of a healthy donor, were incubated with either *CD80*$^{-/-}$*CD86*$^{-/-}$ Raji or *CD80*$^{-/-}$*CD86*$^{-/-}$*CD80-GFP*⁺ Raji, isolated by FACS, and then cultured with mature DCs derived from human monocytes of another donor, in the presence of SEB, before flow cytometry analysis of IL-2⁺ and IFNγ⁺ T cells, summarized in the bar graphs. **(B)** Upper: Experimental scheme depicting the assay setup. Human CD4⁺ T cells, purified from PBMCs, were incubated with either *CD80*$^{-/-}$*CD86*$^{-/-}$ Raji or *CD80*$^{-/-}$*CD86*$^{-/-}$*CD80-GFP*⁺ Raji, to allow for trogocytosis, isolated by FACS, and then cultured for 1–4 d with SEB in the presence or absence of ipilimumab before measurement of IL-2 concentration in the medium. Lower: Plot summarizing IL-2 concentrations in the indicated conditions. Error bars: SD. **, P < 0.01; ***, P < 0.001; unpaired two-tailed Student's *t* test.

contacts. Again, HLA-DR levels were unaffected by CTLA4 or CD28 blockade. Therefore, while bystander acquisition of APC molecules including MHC can occur non-specifically via CD28 or CTLA4-dependent trogocytosis, CTLA4-mediated cis-endocytosis appears to be specific for B7 molecules.

In a parallel set of experiments, we examined whether CTLA4 depletes CD80 in cis on human Tconv cells (CD4⁺CD25^{low} CD127^{high}), analogous to the Treg assays (Fig. 5 C). A similar pattern was observed (Fig. 5 D): CD80 was depleted in a Tconv-intrinsic manner, and CTLA4 blockade, but not CD28 blockade, partly preserved CD80 levels on Tconv cells, though the recovery did not reach statistical significance. Akin to the observation in Tregs, 9 h incubation or CTLA4/CD28 blockade did not affect the HLA-DR levels on the Tconv surface (Fig. 5 D), consistent with specific depletion of B7 molecules by CTLA4.

Because CTLA4 expression and polarization to the cell surface are promoted by TCR stimulation (Egen and Allison, 2002; Linsley et al., 1996), as we confirmed with Treg cells (Fig. S5 A), we next determined whether CTLA4-mediated cis-endocytosis of B7 ligands is regulated by TCR signaling. Indeed, the magnitude of B7 depletion and recovery in response to CTLA4 blockade were much more modest in the absence of SEB than in the presence of SEB (Fig. S5 B). Thus, TCR stimulation promotes CTLA4-mediated cis depletion of CD80 from the cell surface.

Cis depletion of trogocytosed CD80 by CTLA4 from T cell surface

CD4⁺ T cells upregulate endogenous CD80 expression upon stimulation (Azuma et al., 1993); thus, anti-CD80 staining of Tregs can be contributed by both trogocytosed and endogenous CD80. Moreover, CTLA4:CD80 interactions might obscure the anti-CD80 antibody epitope. To more precisely probe trogocytosed vs. endogenous CD80, we engineered Myc-CD80-expressing Raji cells (*CD80*$^{-/-}$*CD86*$^{-/-}$*Myc-CD80*⁺) and used them to precondition Tregs as in Fig. 5. Anti-Myc staining revealed that the acquired Myc-CD80 was depleted considerably from Treg surface in 3 h and blockade of CTLA4, but not of CD28, prevented Myc-CD80 depletion regardless of the presence of filler cells (Fig. 6 A), as seen in Fig. 5 with anti-CD80 staining, supporting the notion that exogenous Myc-CD80 depletion occurred in a largely cell-intrinsic fashion on Tregs. Removal of antigen prevented the Myc-CD80 depletion (Fig. 6 B), further supporting that cis depletion of exogenous CD80 can be promoted by TCR signal. As a validation of specificity, anti-Myc stained Myc-CD80, but not untagged CD80 expressed at a similar level (Fig. 6 C). Moreover, when Myc-CD80 was coexpressed with CTLA4 on Jurkat cells, anti-Myc staining on ice was unaffected by CTLA4 blockade (Fig. 6 D), suggesting that cis-CTLA4:CD80 interaction does not obscure Myc-tag staining. These data demonstrate that CTLA4 depletes trogocytosed CD80 from the Treg surface in cis, likely due to its endolysosomal trafficking mediated by the CTLA4 intracellular domain (ICD; Valk et al., 2008). Consistent with this notion, when expressed at comparable levels on Jurkat cells (Fig. 6 E), CTLA4^{WT}, but not its ICD-deleted mutant CTLA4$^{\Delta ICD}$, mediated depletion of trogocytosed Myc-CD80 from the cell surface, as evidenced by the effects of ipilimumab on anti-Myc staining (Fig. 6 F). Moreover, CTLA4 failed to deplete trogocytosed Myc-CD80 when Jurkat cells were incubated on ice (Fig. 6 F), a condition known to prevent CTLA4 trafficking.

Altogether, data presented in this section further corroborates the model that CTLA4 depletes trogocytosed B7 ligands from the T cell surface through cis-endocytosis in a TCR-promoted manner.

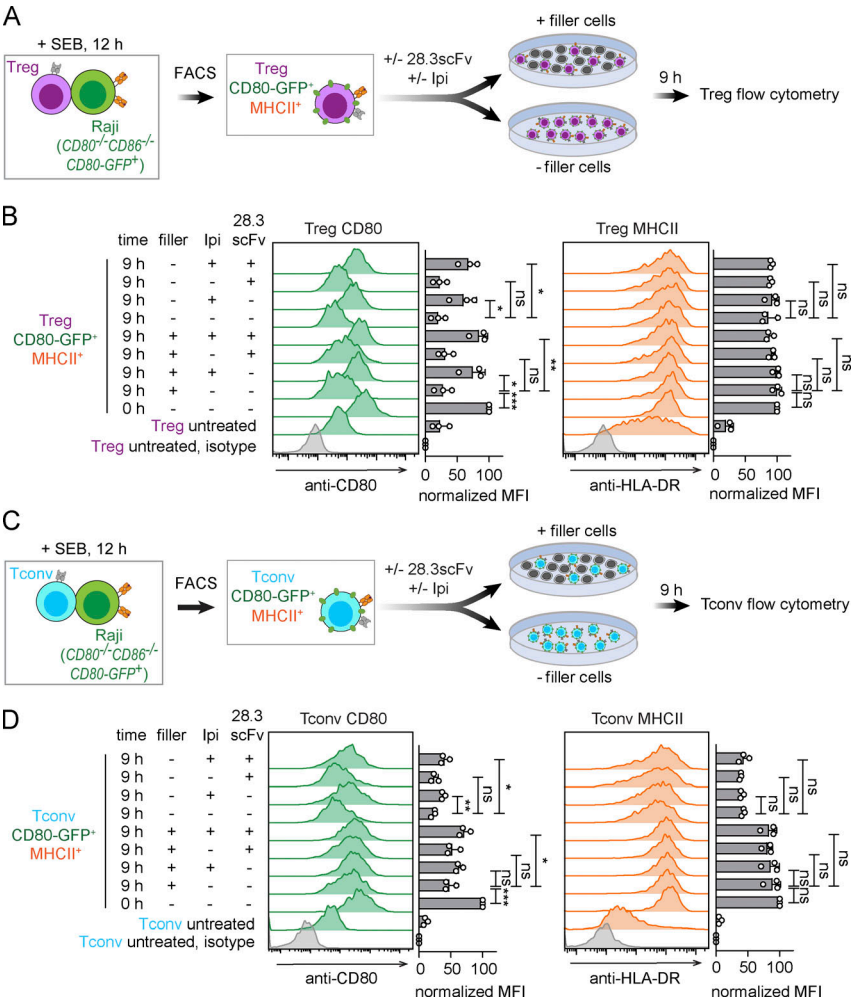

Figure 5. **CTLA4 mediates T cell–intrinsic cis depletion of CD80 but not MHCII. (A)** Experimental scheme. Human Tregs were precultured with *CD80*$^{-/-}$*CD86*$^{-/-}$*CD80-GFP*$^{+}$ Raji cells in the presence of SEB, isolated by FACS, and incubated alone or with 30-fold excess of *CD28*$^{-/-}$ Jurkat filler cells for 9 h, in the presence or absence of ipilimumab and/or 28.3scFv before flow cytometry measurement of CD80 and HLA-DR amounts. **(B)** Representative flow cytometry histograms and quantification graph of CD80 and HLA-DR amounts on Tregs before (0 h) and after 9 h incubation under the indicated conditions. Tregs at 0 h were preconditioned by *CD80*$^{-/-}$*CD86*$^{-/-}$*CD80-GFP*$^{+}$ Raji cells as shown in A. Normalized MFIs of anti-CD80 and anti–HLA-DR were calculated by setting the MFI of "Treg untreated, isotype" condition as 0 and the MFI of "0 h, –, –, –" condition as 100. **(C and D)** Same as A and B except replacing human Tregs with human Tconvs. Error bars are SD from three independent coculture experiments using PBMCs from three independent age-matched donors. *, P < 0.05; **, P < 0.01; ***, P < 0.001; unpaired two-tailed Student's *t* test.

Cis depletion of T cell endogenous CD80 by CTLA4

We then investigated whether CTLA4 can similarly deplete endogenously expressed CD80 from the T cell surface via cis-interactions. To examine CTLA4:B7 cis-interactions, we first asked if coexpression of B7 ligands with CTLA4 can prevent CTLA4 from binding to soluble B7-Ig. We engineered *CD28*$^{-/-}$*CTLA4*$^{\Delta ICD}$-*mCherry*$^{+}$ Jurkat, which expressed mCherry-tagged CTLA4$^{\Delta ICD}$ that localized substantially to the cell surface. As expected, these cells could be stained by soluble CD80-Ig or CD86-Ig (Fig. 7, A and B). Notably, coexpression of either CD80 or CD86 on the aforementioned Jurkat markedly decreased surface staining by B7-Ig, with minimal impact on CTLA4$^{\Delta ICD}$-mCherry expression, based on both microscopy and flow cytometry readouts (Fig. 7, A and B). These data indicate that CTLA4 can interact with T cell endogenous B7 in cis at the cell surface.

To determine if CTLA4 can deplete T cell endogenous CD80 in cis, we stimulated TCR/CD28 signaling in Treg using SEB-pulsed, *CD80*$^{-/-}$*CD86*$^{-/-}$*CD86-GFP*$^{+}$ Raji cells to promote CTLA4 expression. During coculture, Treg also trogocytosed CD86-GFP from Raji, while the CD80 on Tregs was exclusively endogenous due to the lack of CD80 expression on Raji cells. This setup allowed us to specifically examine the CTLA4 regulation of Treg-endogenous CD80. To this end, we isolated Raji (*CD80*$^{-/-}$*CD86*$^{-/-}$*CD86-GFP*$^{+}$)-conditioned Treg cells and examined their CD80 expression during monolayer culture in the presence of 30-fold excess of *CD28*$^{-/-}$ Jurkat filler cells, with or without ipilimumab. In the absence of ipilimumab, endogenous CD80 levels on Treg decreased appreciably following coculture with SEB-loaded *CD80*$^{-/-}$*CD86*$^{-/-}$*CD86-GFP*$^{+}$ Raji cells (Fig. 7 C, "0 h, +, –, –" vs. "Treg untreated"), likely due to TCR-promoted CTLA4-mediated CD80 cis depletion. Consistent with this notion, treatment of ipilimumab, but not 28.3scFv, at 37°C led to a marked increase in CD80 expression on Treg cells, and this effect was much less pronounced on ice (Fig. 7 C). We next validated these results using Jurkat cells coexpressing Myc-CD80 and CTLA4-GFP: ipilimumab-mediated blockade of cis-CTLA4:CD80 interactions in the presence of filler cells increased the cell surface level of Myc-CD80, as shown by anti-Myc staining (Fig. 7 D). In contrast, ipilimumab had little effect on Myc-CD80 staining when the cells were incubated on ice to inhibit endocytosis, or expressed the endocytosis-defective mutant CTLA4$^{\Delta ICD}$ (Fig. 7 D). Thus, CTLA4 depletes T cell endogenous CD80 through cis-endocytosis.

CD80 and CD86 acquired by CD28-dependent trogocytosis accumulate in CTLA4-containing intracellular vesicles over time

Having established that CTLA4 can deplete B7 molecules in cis from the T cell surface, we next asked whether CTLA4-mediated

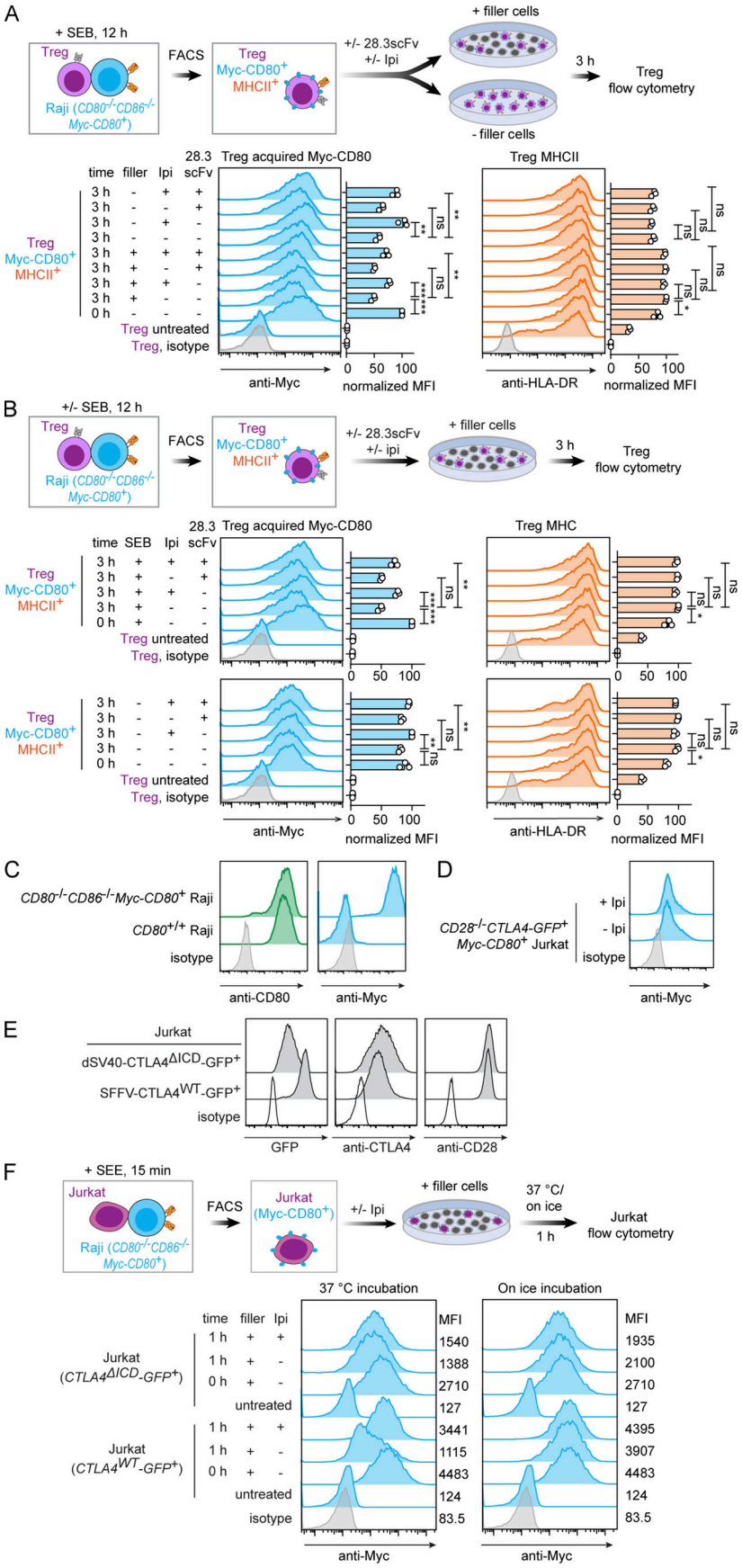

Figure 6. **CTLA4 mediates cis-endocytosis of CD80 acquired via trogocytosis. (A)** Effects of filler cells on CTLA4-mediated depletion of Treg trogocytosed Myc-CD80. Human Tregs were precultured with Myc-CD80–expressing Raji (*CD80*$^{-/-}$*CD86*$^{-/-}$*Myc-CD80*$^{+}$) in the presence of SEB, isolated by FACS, and incubated alone or with 30-fold excess of *CD28*$^{-/-}$ Jurkat filler cells for 0 or 3 h, in the presence or absence of ipilimumab and/or 28.3scFv before flow cytometry measurement of Myc-CD80 and HLA-DR amounts. Bar graph summarizes data from three technical replicates of Tregs isolated from a single human donor. **(B)** Effect of TCR stimulation on CTLA4-mediated cis depletion of Treg trogocytosed Myc-CD80. Tregs were precultured with Myc-CD80–expressing Raji (*CD80*$^{-/-}$*CD86*$^{-/-}$*Myc-CD80*$^{+}$) in the presence or absence of SEB, isolated by FACS, and incubated with 30-fold excess of *CD28*$^{-/-}$ Jurkat filler cells for 0 or 3 h, in the presence or absence of ipilimumab and/or 28.3scFv before flow cytometry measurement of Myc-CD80 and HLA-DR. Bar graph summarizes data from three technical replicates of Tregs isolated from a single human donor. **(C)** Flow cytometry histograms showing Myc-CD80 and endogenous CD80 expression on indicated Raji cells measured by anti-CD80 staining and anti-Myc staining, respectively. **(D)** Flow cytometry histograms of anti-Myc staining of indicated Jurkat cells in the presence or absence of ipilimumab. **(E)** Flow cytometry histograms showing the GFP signal (total expression of CTLA4), anti-CTLA4 staining (surface expression of CTLA4), and anti-CD28 staining (surface expression of CD28) on indicated Jurkat cells. **(F)** Ipilimumab effects on the cell surface expression of trogocytosed Myc-CD80 in Jurkat expressing CTLA4^{WT} or CTLA4$^{\Delta ICD}$. Flow cytometry histograms show anti-Myc staining of indicated Jurkat after 1 h incubation in the presence of excess filler cells at 37°C or on ice, with or without ipilimumab. In A and B, normalized MFIs were calculated by setting the absolute 0 as 0 and the highest MFI value among all the conditions as 100 in each replicate. Error bars: SD. *, P < 0.05; **, P < 0.01; ***, P < 0.001; unpaired two-tailed Student's *t* test.

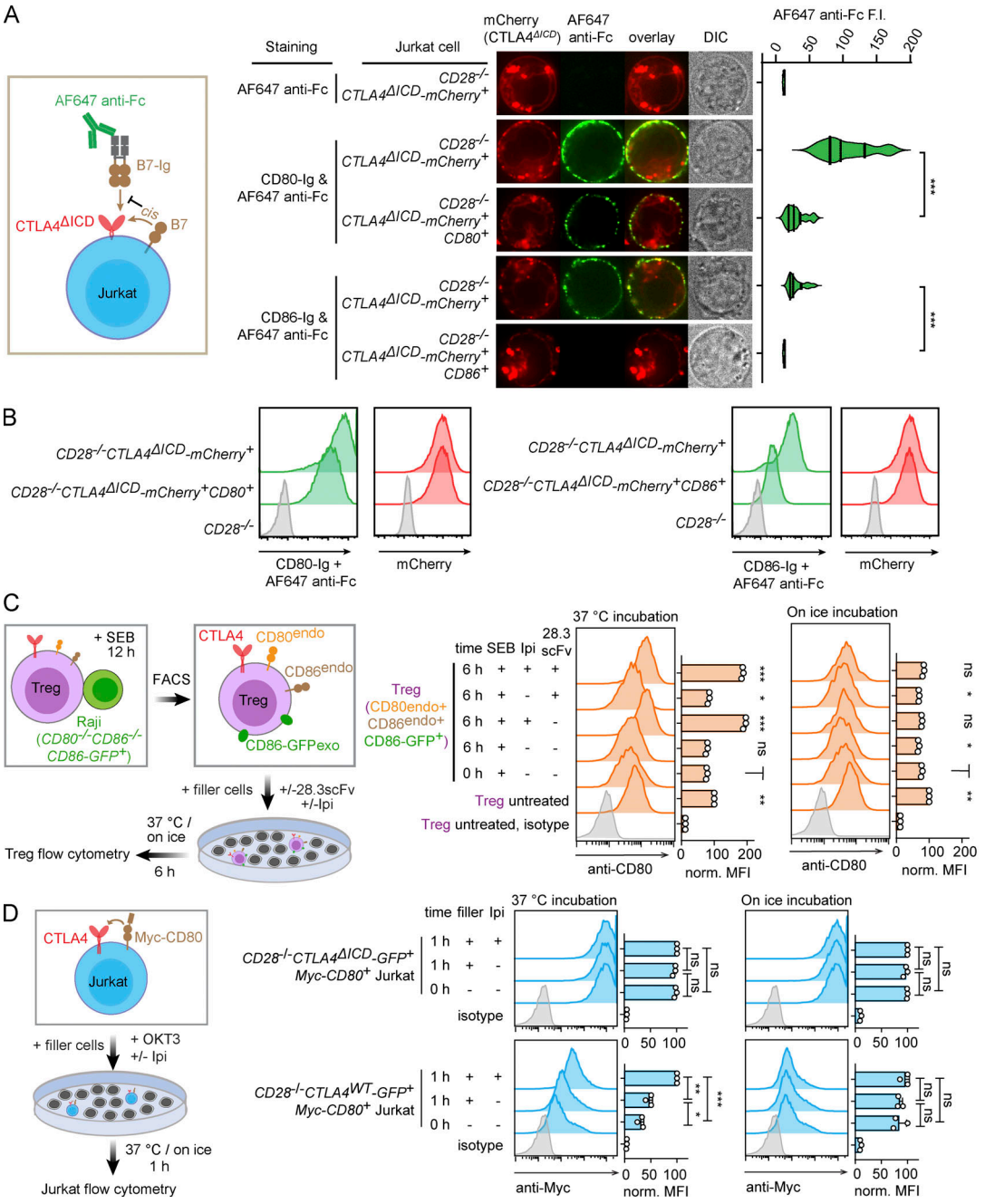

Figure 7. **CTLA4 binds and depletes T cell–intrinsic CD80 in cis. (A)** Left: Experimental scheme. Right: Representative confocal images and quantification violin plot showing how coexpression of CD80 or CD86 affected the B7-Ig staining of CTLA4$^{\Delta ICD}$. **(B)** Flow cytometry histograms showing how coexpression of CD80 or CD86 affected the B7-Ig staining of CTLA4$^{\Delta ICD}$. **(C)** CTLA4 regulation of endogenous CD80 expression on human Tregs. Human Tregs were precultured with *CD80*$^{-/-}$*CD86*$^{-/-}$*CD86-GFP*$^{+}$ Raji, isolated by FACS, and incubated with 30-fold excess of *CD28*$^{-/-}$ Jurkat filler cells for 6 h, in the presence or absence of ipilimumab and/or 28.3scFv before flow cytometry measurement of anti-CD80 staining. Data presented as three technical replicates for Tregs from a single human donor (male, age 30). Normalized MFIs were calculated by setting the absolute 0 as 0 and the MFI of "Treg untreated" condition as 100 in each replicate. **(D)** CTLA4 regulation of Myc-CD80 expression in Jurkat cells. *CD28*$^{-/-}$ or *CD28*$^{+/+}$ Jurkat cells cotransduced with CTLA4 and Myc-CD80 were incubated with a 30-fold excess of *CD28*$^{-/-}$ Jurkat filler cells for 1 h, in the presence or absence of ipilimumab before flow cytometry measurement of anti-Myc staining. Normalized MFIs were calculated by setting the absolute 0 as 0 and the highest MFI value among all the conditions as 100 in each replicate. Error bars: SD. *, P < 0.05; **, P < 0.01; ***, P < 0.001; unpaired two-tailed Student's *t* test.

B7 cis depletion can act downstream of CD28-mediated B7 trogocytosis. To this end, we visualized the subcellular localization of CD28, CTLA4, and B7 after CD28-mediated B7 trogocytosis in isolated single T cells. To enable three-color imaging, we coexpressed CTLA4-mCherry and CD28 fused with SpyTag (Spy-CD28) in *CD28*$^{-/-}$ Jurkat cells and labeled Spy-CD28 covalently with recombinant SpyCatcher (Zakeri et al., 2012) conjugated with a far-red fluorophore JF646. After a brief incubation of

JF646-Spy-CD28$^+$*CTLA4-mCherry*$^+$*CD28*$^{-/-}$ Jurkat with *CD80-GFP*$^+$ Raji cells to induce trogocytosis of CD80-GFP, we immediately isolated GFP$^+$/JF646$^+$/mCherry$^+$ Jurkat cells and cultured them at a low density to limit T–T contacts (Fig. 8 A). Confocal imaging showed that upon acquisition, CD80-GFP initially coclustered with CD28 at the plasma membrane, but not with CTLA4-mCherry, which was localized to intracellular vesicles as expected (Fig. 8 B, 0 min). However, images captured at later time points revealed a progressive accumulation of CTLA4 at sites of acquired APC-derived fragments and a concomitant accumulation of CD80-GFP within CTLA4$^+$ vesicles (Fig. 8 B, "15–120 min"). Ipilimumab treatment significantly inhibited the accumulation of CD80-GFP in CTLA4$^+$ vesicles (Fig. 8 B, "120 min, +ipi"). In a parallel set of experiments, we found that trogocytosed CD86 exhibited a similar pattern of localization: initially colocalizing with CD28 at the plasma membrane before becoming associated with CTLA4 over time in a manner that could be inhibited by ipilimumab treatment (Fig. 8, C and D). Next, we sought to verify the vesicular colocalization of CTLA4 and B7 using EM in human primary T cells. We transduced human CD4$^+$ T cells with CTLA4-HaloTag. After 15 min incubation of these cells with Raji (*CD80-GFP*$^+$) to induce trogocytosis and a further 1 h incubation to allow CTLA4-mediated internalization, we then fixed the cells and labeled CTLA4-HaloTag via photo-oxidation and CD80 using immunogold (Fig. 8 E). Consistent with light microscopy shown above, electron micrographs revealed the presence of CD80 within CTLA4-associated vesicles (Fig. 8 F).

Altogether, these data demonstrate that CTLA4-mediated cis-endocytosis can act downstream of CD28-mediated trogocytosis to internalize acquired B7 molecules from the cell surface.

Both CD28 and CTLA4 contribute to human Treg-mediated trans depletion of B7 from APCs

Our data support a model in which CTLA4-mediated B7 cis-endocytosis can efficiently operate downstream of ligand acquisition via trogocytosis induced by CD28:B7 binding. This mechanism therefore led us to test the prediction that CD28 contributes substantially to the phenomenon of trans depletion of B7 from APCs by Treg, a process previously described to be mediated by trans-endocytosis and solely CTLA4 dependent (Qureshi et al., 2011). Here, we aimed to determine the potential contribution of ligand acquisition via CD28 and subsequent cis-endocytosis by CTLA4 in mediating processive B7 depletion using human Tregs.

We first cocultured human Tregs with *CD80-GFP*$^+$ Raji or with *CD86-GFP*$^+$ Raji in the presence or absence of SEB, with or without 28.3scFv or ipilimumab (Fig. 9 A). To examine B7 depletion from APCs, we monitored CD80 levels on Raji APCs rather than on T cells. Upon 9 h of coculture with human Tregs in the presence of SEB, CD80-GFP signal in Raji cells decreased by ∼60% (Fig. 9 B, "+, +, –, –"), consistent with prior reports that Tregs induce CD80 depletion from APCs in a contact-dependent manner. As expected, CD80-GFP trans depletion from Raji cells was sharply inhibited by ipilimumab (Fig. 9 B, "+, +, +, –"). Notably, however, the presence of 28.3scFv also inhibited CD80-GFP depletion to a similar extent as that of CTLA4 blockade (Fig. 9 B, "+, +, –, +"). This result uncovers a previously unappreciated role of CD28 in CD80 depletion from APCs by Tregs, consistent with a processive "two-step" mechanism involving ligand acquisition via CD28-dependent trogocytosis followed by CTLA4-mediated cis-endocytosis. When both ipilimumab and 28.3scFv were present, CD80-GFP depletion from Raji was further abrogated (Fig. 9 B, "+, +, +, +"), suggesting a synergy of CD28 and CTLA4 in Treg-mediated B7 depletion. Weaker CD80-GFP depletion was observed in the absence of SEB (Fig. 9 B, +Treg/–SEB conditions), consistent with the TCR-promoted cis depletion of B7, as observed in Fig. 6 B and Fig. S5. Under these conditions, either CD28 or CTLA4 blockade again inhibited B7 depletion from Raji cells, as observed in the presence of SEB. Thus, CD28-mediated trogocytosis cooperates with CTLA4 to facilitate Treg-mediated depletion of CD80 from APCs.

In parallel, we also examined the role of CD28 and CTLA4 in Treg-mediated depletion of CD86-GFP from Raji (*CD86-GFP*$^+$) cells. Akin to CD80 depletion experiments, either CD28 or CTLA4 blockade attenuated Treg-mediated CD86-GFP depletion from Raji APCs, with CD28 blockade displaying an even greater effect than CTLA4 blockade (Fig. 9 C). This result highlights the novel role of CD28-dependent trogocytosis in facilitating trans depletion of APC B7 by Treg cells.

Altogether, data presented in this section support a model in which CD28-dependent trogocytosis coupled with CTLA4-mediated cis-endocytosis of B7 ligands can act synergistically to facilitate the processive acquisition, display, and specific depletion of APC-derived B7 but not associated MHC molecules by human Treg cells.

Discussion

B7 costimulatory ligands are best known to be upregulated by professional APCs in response to pathogens or inflammation to provide the essential "second signal" of T cell activation via CD28. However, these ligands are also displayed by T cells themselves through both trogocytosis and endogenous expression (Azuma et al., 1993; Sabzevari et al., 2001; Trzupek et al., 2020). Increasing evidence supports the functional significance of T cell B7 ligands, including trans-activating CD28 on other T cells, as well as cis-activating CD28 on the same T cells as we showed recently (Zhao et al., 2023). Here, we report that the levels of B7 ligands displayed by human T cells can be restricted by CTLA4-dependent cis-endocytosis (Fig. 10). Accordingly, ipilimumab treatment increases T cell autostimulation by promoting T cell display of costimulatory information. This pathway may therefore contribute to both the therapeutic benefit and adverse effects associated with CTLA4-targeted therapies.

While CD28 mediates costimulatory signaling upon binding to B7 ligands, data presented here and previously support an additional role of CD28 in mediating the acquisition and redisplay of APC-derived membrane fragments and associated surface molecules, including B7 ligands and peptide antigen (MHC; Hwang et al., 2000; Sabzevari et al., 2001; Tatari-Calderone et al., 2002; Zenke et al., 2022). This process of membrane transfer endows resultant MHC$^+$/B7$^+$ T cells with the capacity to autostimulate in the absence of APCs and may enable T cells to

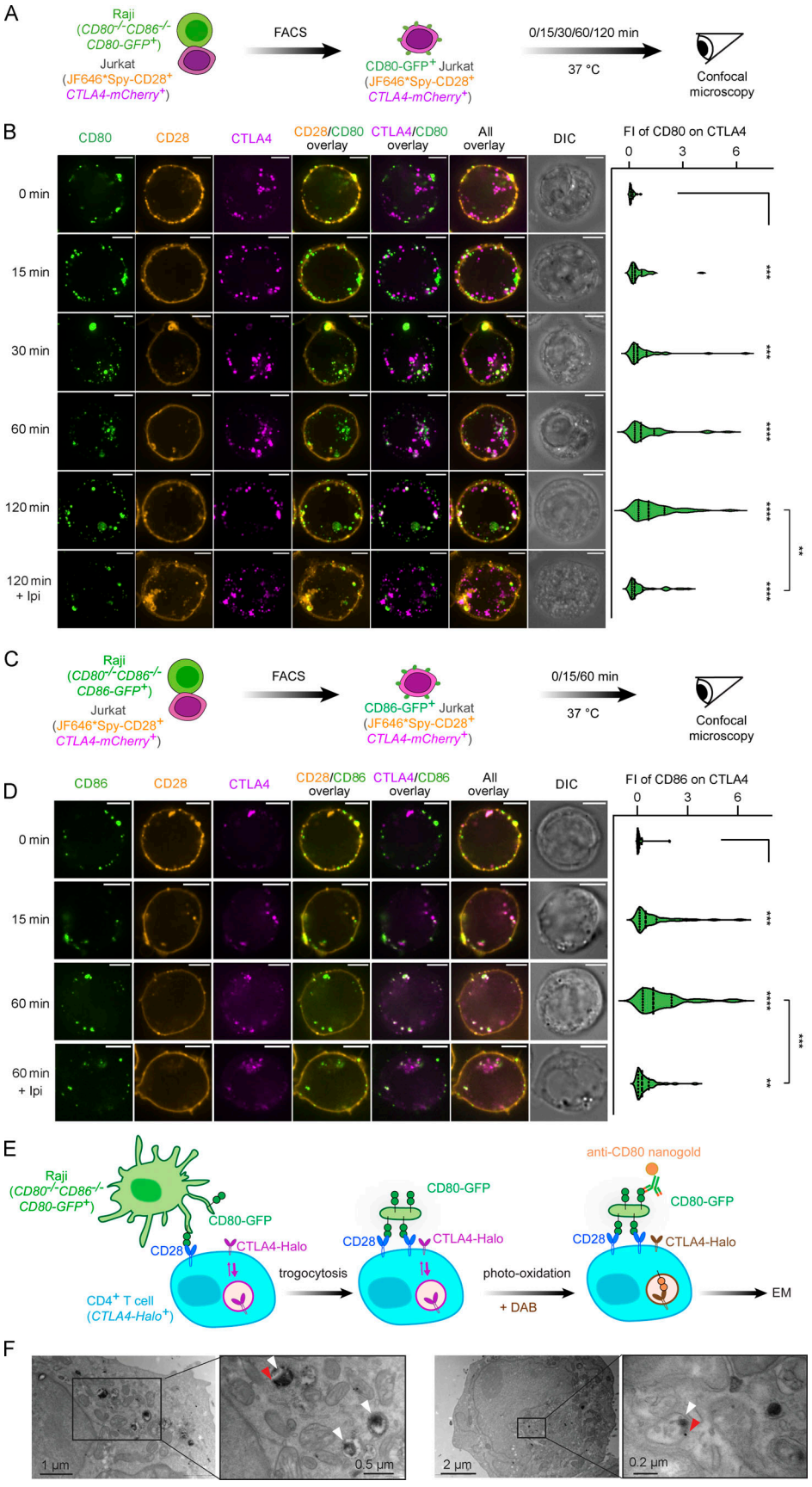

Figure 8. **B7 ligands acquired by trogocytosis initially colocalize with CD28 prior to subsequent cis capture and internalization by CTLA4. (A)** Experimental scheme for examining the localization of trogocytosed CD80 in Jurkat cells. After coculture with *CD80*$^{-/-}$*CD86*$^{-/-}$*CD80-GFP*$^{+}$ Raji cells, Jurkat (JF646-

SPY-CD28$^+$*CTLA4-mCherry*$^+$) cells were isolated, incubated alone or in the presence of ipilimumab for indicated durations, fixed, and imaged for CD80-GFP, CD28, and CTLA4. **(B)** Left: Representative maximum intensity z-projection confocal micrographs showing the CD28/CD80/CTLA4 localizations in CD80-GFP acquired Jurkat (JF646-SPY-CD28$^+$*CTLA4-mCherry*$^+$) cells at indicated time points of post-sorting incubation. Right: A violin plot showing the relative FI values of CD80-GFP colocalized with CTLA4. **(C and D)** Same as A and B except replacing CD80-GFP with CD86-GFP and showing single images instead of maximum intensity z-projection images. **(E)** Cartoon depicting dual EM labeling strategy using CD4$^+$ T cells expressing CTLA4-HaloTag conjugated with *CD80*$^{-/-}$*CD86*$^{-/-}$*CD80-GFP*$^+$ Raji cells. Laser excitation at 549 nm induces oxidative polymerization of electron-dense DAB proximal to CTLA4-HaloTag (JFX-549), CD80 was labeled by 10-nm nanogold conjugated secondary antibody. **(F)** Electron micrographs showing CTLA4-HaloTag (DAB staining, white arrowheads) and CD80 (nanogold, red arrowheads). Scale bar: 5 µm. Error bars are SD from 40 cells. **, P < 0.01; ***, P < 0.001; ****, P < 0.0001; unpaired two-tailed Student's *t* test.

collectively establish a coherent "quorum" of similarly responding clones. Indeed, the presence or absence of T cell quorum has been proposed as an alternative model for CD4$^+$ helper subset polarization and peripheral "self"/non-self-discrimination (Al-Yassin and Bretscher, 2018; Bretscher, 2014a; Bretscher, 2014b; Butler et al., 2013; Rudulier et al., 2014).

Whether CTLA4 functions in a cell-extrinsic or -intrinsic manner has been debated. The cell-extrinsic function of CTLA4 is best documented in the context of Tregs, which downregulate B7 on professional APCs in a CTLA4- and contact-dependent manner. Specifically, the trans-endocytosis model of CTLA4 function has been proposed to account for trans depletion of B7 and the ability of Tregs to dominantly control CTLA4-deficient T cells in a cell-extrinsic manner (Hou et al., 2015). Here, we uncover a role for CD28-dependent trogocytosis in this trans-depletion process. Our data support a two-step mechanism in which CD28-mediated B7 trogocytosis can operate upstream of CTLA4-mediated cis depletion of B7 from the T cell surface. Notably, despite inducing rapid acquisition of B7-containing membrane fragments, CD28 alone was unable to efficiently deplete B7 (Fig. 5). We suggest that acquired B7 ligands may locally saturate CD28 in the absence of CTLA4, which can act as a molecular sink to deplete B7 in cis and thereby desequester CD28 for additional rounds of ligand transfer. This two-step process would thus facilitate processive, multiround trogocytosis of B7 for efficient depletion from B7-abundant APCs.

While our data suggest CD28 as the predominant mediator of B7 ligand acquisition, consistent with its substantially higher cell-surface expression than CTLA4, we found that CTLA4 is also capable of inducing B7 trogocytosis when highly expressed in CD28-deficient T cell lines. Therefore, it is likely that at high surface levels, CTLA4 itself can trans-deplete B7 molecules through an analogous two-step mechanism comprised of trogocytosis followed by cis-endocytosis. Indeed, CTLA4:B7 binding was similarly associated with bystander transfer and redisplay of MHC molecules (Fig. 3), consistent with a trogocytosis mechanism as recently suggested for CTLA4 (Tekguc et al., 2021) rather than direct trans-endocytosis. The contribution of CTLA4 in trans-acquisition of APC-derived B7/MHC relative to CD28 likely varies depending on its surface expression, which is limited by its highly endocytic nature but promoted by TCR stimulation.

The ability of CTLA4 to deplete B7 molecules in cis from both human Tregs and Tconvs (Fig. 5) highlights a novel T cell–intrinsic function of CTLA4. This function is consistent with its continuous recycling, lysosomal trafficking, and high affinity to B7 ligands that would allow efficient capture of either free or CD28-bound B7. The observed TCR promotion of CTLA4 cis-endocytosis likely facilitates TCR-dependent control of B7

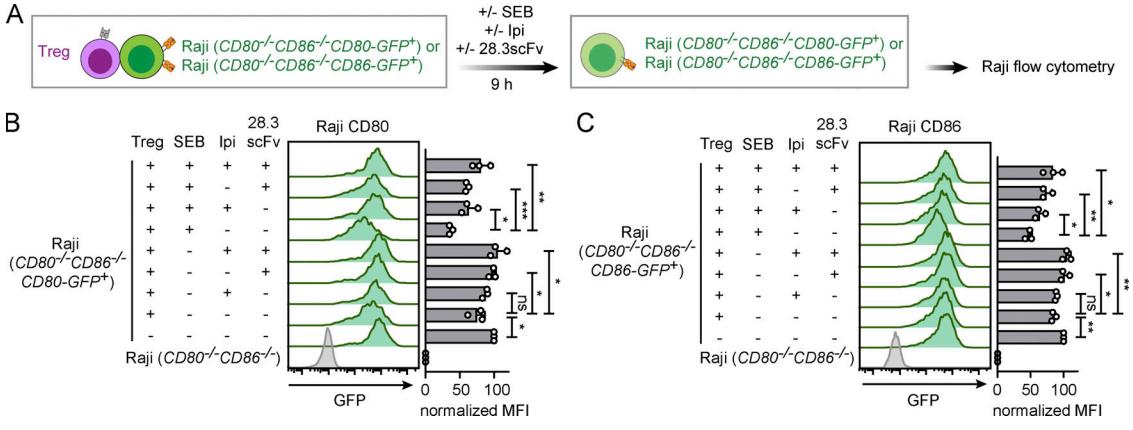

Figure 9. **Blockade of either CD28 or CTLA4 inhibits B7 depletion from APCs by human Tregs. (A)** Schematics of a Treg:Raji coculture assay examining Treg-mediated depletion of B7 ligands from APCs. GFP fluorescence in Raji (*CD80*$^{-/-}$*CD86*$^{-/-}$*CD80-GFP*$^+$) or Raji (*CD80*$^{-/-}$*CD86*$^{-/-}$*CD86-GFP*$^+$) cells was measured by flow cytometry after 9 h coculture with human Tregs. **(B)** Representative flow cytometry histograms and quantification graph of CD80-GFP amounts in Raji (*CD80*$^{-/-}$*CD86*$^{-/-}$*CD80-GFP*$^+$) after incubation with Tregs under the indicated conditions. Normalized MFIs of CD80-GFP were calculated by setting the MFI of Raji (*CD80*$^{-/-}$*CD86*$^{-/-}$) as 0 and the MFI of "–, –, –, –" as 100. **(C)** Same as B except measuring CD86-GFP in Raji (*CD80*$^{-/-}$*CD86*$^{-/-}$*CD86-GFP*$^+$) cells. Error bars are SD from three independent coculture experiments using PBMCs from three independent age-matched donors. *, P < 0.05; **, P < 0.01; ***, P < 0.001; unpaired two-tailed Student's *t* test.

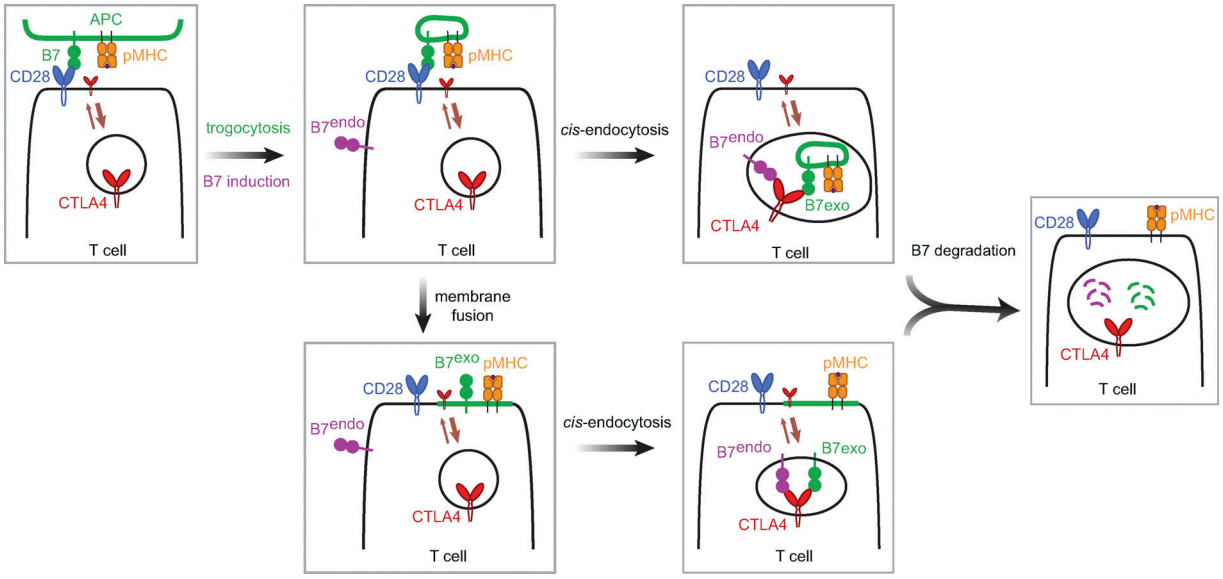

Figure 10. **Proposed working model.** Summary of the proposed working model of CD28-mediated trogocytosis of B7 ligands from APCs followed by CTLA4-mediated cis-endocytosis of acquired B7 from the T cell surface.

ligand availability via a CTLA4-mediated negative feedback mechanism to regulate costimulatory signaling and thereby maintain immune homeostasis. Notably, only B7 ligands, but not MHC, are depleted in cis by CTLA4. Thus, the cell-intrinsic action of CTLA4 might contribute to the generation of MHC^{+}/B7^{low} T cells with tolerogenic activity as recently suggested for Treg displaying trogocytosed pMHC (Akkaya and Shevach, 2020).

Mechanistically, CTLA4 cis-endocytosis of endogenous B7 may proceed as a direct consequence of their cis-interaction due to the highly endocytic feature of CTLA4. As CTLA4 binds to B7 with high affinity, their cis-interaction might also invaginate the underlying plasma membrane to promote endocytosis. CTLA4 cis-endocytosis of exogenous B7 might occur either through directly displacing CD28 at the interface between a T cell and a discrete membrane fragment held at the cell surface, or through cis-capture of B7 if the trogocytosed membrane has fused with the recipient T cell (Fig. 10). This cell-intrinsic action would enable CTLA4 to limit the amount and duration that costimulatory information is displayed on T cell surface. Distinct from the trans-endocytosis model, which requires durable contact between Tregs and professional APCs to extrinsically regulate subsequent T cell:APC interactions, the T cell–intrinsic model proposed here represents an independent route for CTLA4 to exert dual intrinsic/extrinsic regulatory function within networks of responding lymphocytes that are not limited to high CTLA4-expressing Tregs. Thus, the present work suggests a spatiotemporal extension of CTLA4 regulatory function from the APC:T cell interface to within T cell populations.

Limitations of the study

We offer evidence that CTLA4 regulates T cell display of costimulatory ligands through cis-endocytosis. Although this model is supported by data from human CD4^{+} T cells, we have not examined this model in CD8^{+} T cells. Additionally, an in vivo test of this model is currently lacking and warrants further investigation.

Materials and methods

Cell lines and cultures

Jurkat E6.1 cells were obtained from Dr. Arthur Weiss (University of California, San Francisco, San Francisco, CA, USA); HEK293T cells and Raji cells from Dr. Ronald Vale (University of California, San Francisco, San Francisco, CA, USA); and HEK293F cells from Dr. Andrew Ward (Scripps Research, San Diego, CA, USA). Jurkat (*CD28*$^{-/-}$) line, Raji (*CD80*$^{-/-}$*CD86*$^{-/-}$) line, Raji (*CD80*$^{-/-}$*CD86*$^{-/-}$*CD80-GFP*$^{+}$) line, and Raji (*CD80*$^{-/-}$*CD86*$^{-/-}$*CD86-GFP*$^{+}$) line were generated in our previous study (Zhao et al., 2019). Jurkat (*CD28*$^{+/+}$CTLA4-Cherry^{high}), Jurkat (*CD28*$^{-/-}$*CD28-Cherry*$^{+}$), Jurkat (*CD28*$^{-/-}$CTLA4-Cherry^{high}), Jurkat (*CD28*$^{+/+}$*CTLA4*$^{\Delta ICD}$*-GFP*$^{+}$), Jurkat (*CD28*$^{+/+}$*CTLA4-GFP*$^{+}$), Jurkat (*CD28*$^{-/-}$*CTLA4*$^{\Delta ICD}$*-mCherry*$^{+}$), and Jurkat (*CD28*$^{-/-}$*Spy-CD28*$^{+}$CTLA4-Cherry^{low}) were generated by lentivirally transducing *CD28*$^{+/+}$ Jurkat E6.1 or *CD28*$^{-/-}$ Jurkat with the indicated fusion genes. Expression of all the genes transduced was driven by the SFFV promoter except for CTLA4-Cherry^{low} and CTLA4$^{\Delta ICD}$-GFP, which was driven by the dSV40 promoter. CTLA4$^{\Delta ICD}$ was generated by deleting aa188–223 from full-length CTLA4. Jurkat (*CD28*$^{-/-}$*CTLA4*$^{\Delta ICD}$*-mCherry*$^{+}$*CD80*$^{+}$), Jurkat (*CD28*$^{-/-}$*CTLA4*$^{\Delta ICD}$*-mCherry*$^{+}$*CD86*$^{+}$), Jurkat (*CD28*$^{-/-}$*CTLA4*$^{\Delta ICD}$*-GFP*$^{+}$*Myc-CD80*$^{+}$), and Jurkat (*CD28*$^{-/-}$*CTLA4-GFP*$^{+}$*Myc-CD80*$^{+}$) were generated by lentivirally transducing the indicated *CD80* or *CD86* genes to the *CD28*$^{-/-}$ Jurkat expressing the indicated CTLA4 gene. Raji (*CD80*$^{-/-}$*CD86*$^{-/-}$*Myc-CD80*$^{+}$) line was generated by lentivirally transducing *Myc-CD80* to Raji (*CD80*$^{-/-}$*CD86*$^{-/-}$) line. HEK293T cells were maintained in DMEM medium (#25-501; Genesee Scientific) supplemented with 10% fetal bovine serum (#FB-02; Omega Scientific) and 1% 100× penicillin–streptomycin

(#SV30010; GE Healthcare) at 37°C/5% CO_2. HEK293F cells were maintained in FreeStyle 293 Expression Medium (#12338-018; Gibco). Jurkat and Raji cells, authenticated by ATCC using short tandem repeats profiling, were maintained in RPMI-1640 medium (#10-041-CM; Corning) supplemented with 10% fetal bovine serum, 100 U/ml of penicillin, and 100 µg/ml of streptomycin at 37°C/5% CO_2. The absence of mycoplasma contamination in the cell lines was verified using PCR Mycoplasma Detection Kit (#G238; Applied Biological Materials Inc.). Immortalized cell lines used in the present study were used within 10 passages from thawing. Tconv and Treg cells were purified from PBMCs of human donors (25–35 yr old) obtained from the San Diego Blood Bank using Mojosort Human CD4 T Cell Isolation Kit and Dynabeads Regulatory $CD4^+/CD25^+$ T Cell Kit (#11363D; Thermo Fisher Scientific). Purified Tconv cells were maintained in a complete RPMI 1640 medium containing 50 µM β-mercaptotethanol and 100 U/ml IL-2 in the presence of Dynabeads Human T-Activator CD3/CD28 (#11132D; Thermo Fisher Scientific). Purified Treg cells were maintained in a complete RPMI-1640 medium containing 50 µM β-mercaptotethanol, 100 nM rapamycin, and 300 U/ml IL-2 in the presence of Dynabeads Human Treg Expander (#11129D; Thermo Fisher Scientific).

Lentiviral transductions

Each gene of interest was introduced into Jurkat cells via lentiviral transduction, as described previously (Xu et al., 2020). Briefly, each cDNA was cloned into a pHR vector backbone and cotransfected with envelop plasmid pMD2.G and packaging plasmid psPAX2 into HEK293T cells using polyethylenimine (#NC1014320; PEI; Thermo Fisher Scientific). Virus-containing supernatants were harvested at 60–72 h after transfection. Jurkat cells were resuspended with the desired virus supernatant, centrifuged at 35°C, 1,000 ×*g* for 30 min, and incubated overnight at 37°C, 5% CO_2; 24 h later, the virus supernatant was replaced with complete RPMI-1640 medium. Cells were further cultured for at least 3 d before sorting/analyses.

Recombinant proteins

MBP-anti-CD28 scFv (28.3scFv) was expressed with a C-terminal His_6 tag in HEK293F cells using the pPPI4 vector. The protein secreted to the culture medium was captured using Ni-NTA agarose (#88223; Thermo Fisher Scientific) in a low imidazole buffer (50 mM Hepes-NaOH, pH 7.5, 150 mM NaCl, 5 mM imidazole, 0.5 mM Tris(2-carboxyethyl)phosphine [TCEP]) and eluted with a high imidazole buffer (50 mM Hepes-NaOH, pH 7.5, 150 mM NaCl, 500 mM imidazole, 0.5 mM TCEP). Eluted protein was then subjected to gel filtration chromatography using storage buffer (50 mM Hepes-NaOH, pH 7.5, 150 mM NaCl, 10% glycerol, and 0.5 mM TCEP). The monomer fractions were pooled, snap-frozen, and stored at −80°C in small aliquots. Gel filtration standards (#1511901; Bio-Rad) were run to confirm the sizes of the eluted protein. Protein concentration was determined by Coomassie-blue-stained SDS-PAGE using known concentrations of bovine serum albumin (#23210; Thermo Fisher Scientific) as the standard.

EM

1 million Jurkat and 1 million Raji cells were induced to form contacts by centrifugation at 300 ×*g* for 1 min and incubated at 37°C for 15 min prior to dissociation by pipetting. Following the trogocytosis assay, cells were seeded on 35-mm glass-bottomed gridded dishes (MatTek), washed in PBS, and fixed in 4% (vol/vol) paraformaldehyde (PFA; Electron Microscopy Sciences) for 15 min at room temperature. Confocal images were acquired using a Zeiss Airyscan confocal microscope with a 63× oil objective. Brightfield (BF) tile scan images were acquired to record the dish grid coordinates and position of cells of interest within this region. Cells were then postfixed in 2.5% (vol/vol) glutaraldehyde (Electron Microscopy Sciences) and 2% (wt/vol) reduced osmium tetroxide. Cells were then dehydrated and embedded using standard protocols. After embedding, the grid pattern of the dish was evident on the blockface and a razor was used to trim the block around the region of interest, which was recorded from BF imaging. 70-nm sections were cut using a diamond knife (Diatome) and imaged on a Zeiss Libra TEM at 120 kV.

For experiments using photo-oxidation, cells were cocultured to induce trogocytosis and seeded on Matek dishes as described following incubation with 50 nM JFX549 ligand for 30 min to label CD80/CTLA4-HaloTag. After fixation, cells were incubated with 0.12% (wt/vol) DAB and immediately photo-oxidized using 561 nm excitation, which was confirmed by the presence of dark precipitate via BF imaging. DAB was removed and cells were postfixed and embedded as described. For anti-CD80 immunogold labeling, cells were fixed in 4% PFA and permeabilized in 0.1% saponin before incubating with anti-CD80 primary antibody (Proteintech, #66406-1-Ig) followed by 10 nm gold conjugated secondary antibody (Ted Pella, #17110-1). Oxidation and embedding was performed as described above.

Jurkat:Raji conjugation followed by confocal microscopy

0.1 million Raji (*CD80*$^{-/-}$*CD86*$^{-/-}$*CD80-GFP*$^+$) cells were pretreated with 30 ng/ml SEE before mixing with 0.1 million Jurkat (*CD28*$^{-/-}$*CD28-mCherry*$^+$) cells and centrifuged at 300 ×*g* for 1 min to initiate cell:cell contact, after which the cocultures were immediately transferred to a 37°C water bath and incubated for 5 min. Cells were gently resuspended and fixed with 2% PFA for 15 min at room temperature. Fixed cells were loaded into a 96-well glass-bottom plate (#P96-1.5H-N; Cellvis) for confocal microscopy assays. Images containing Jurkat:Raji conjugates were acquired with a Nikon spinning-disk confocal microscope, then processed and quantified using Fiji (Schindelin et al., 2012). To quantify the CD28 enrichment in the Jurkat:Raji interface, CD28 (mCherry) mean fluorescence intensity (MFI) in the Jurkat:Raji interface was quantified and divided by the CD28 (mCherry) MFI outside of the interface for each conjugate. Representative images from 20 individual Jurkat:Raji cell conjugates were quantified for each sample.

Trogocytosis assays for measuring CD80/CD86 acquisition by Treg, Tconv, and Jurkat cells

Human Treg cells, human Tconv cells, or Jurkat cells were suspended in a complete RPMI medium containing no blocking

agents, 100 µg/ml ipilimumab, 20 µg/ml MBP-28.3scFv, or 100 µg/ml ipilimumab and 20 µg/ml MBP-28.3scFv combined, and incubated for 30 min at 37°C. Indicated Raji cells were prestained with VF405 (#30068-T; Biotium) before being resuspended in complete RPMI medium containing no antigen, 500 ng/ml SEB, or 3 ng/ml SEE for 30 min at 37°C. Afterward, 0.2 million of each type of the aforementioned Raji cells and 0.4 million of each type of the pretreated Treg, Tconv, or Jurkat cells were mixed and centrifuged at 300 ×*g* for 1 min to initiate cell: cell contact, after which the cocultures were immediately transferred to a 37°C water bath. 15 min later, cocultures were resuspended in ice-cold PBS and subjected to flow cytometry analysis of GFP signal, or fixed and stained with anti-CD80, anti-CD86, or anti-HLA-DR antibodies before flow cytometry analysis or cell sorting of VF405 negative cells.

Coculture assays for measuring Treg-mediated CD80/CD86 trans depletion from Raji APCs

Human Treg cells were preincubated in complete RPMI medium containing no blocking agents, 100 µg/ml ipilimumab, 20 µg/ml MBP-28.3scFv, or 100 µg/ml ipilimumab and 20 µg/ml MBP-28.3scFv combined for 30 min at 37°C. Indicated Raji cells were prestained with VF405 before being resuspended in complete RPMI medium containing no antigen or 500 ng/ml SEB for 30 min at 37°C. Afterward, 0.2 million of each type of the aforementioned Raji cells and 0.4 million of each type of the pretreated Treg cells were mixed and centrifuged at 300 ×*g* for 1 min to initiate cell:cell contact, after which the cocultures were immediately transferred to a 37°C water bath and incubated for 5 min. After an additional 9 h incubation in a 37°C/5% CO2 incubator, cocultures were resuspended in ice-cold PBS and subjected to flow cytometry analysis of GFP signal, or fixed and stained with anti-CD80, anti-CD86, or anti–HLA-DR antibodies before flow cytometry analysis or cell sorting of VF405 positive cells.

Cell-intrinsic depletion of CD80 and CD86 in Treg, Tconv, and Jurkat cells

Treg, Tconv, or Jurkat cells were stained with VF405. Indicated Raji cells were preincubated in complete RPMI medium containing no antigen, 500 ng/ml SEB, or 3 ng/ml SEE for 30 min at 37°C. Afterward, 5 million of each type of the aforementioned Raji cells and 10 million of the pretreated Treg, Tconv, or Jurkat cells were mixed in 7.5 ml complete RPMI medium containing no antigen, 100 ng/ml SEB, or 3 ng/ml SEE as indicated, and cultured for 12 h (for Treg and Tconv) or 15 min (for CTLA4 expressing Jurkat) in a 37°C/5% CO_2 incubator. Cocultures were spun down at 300 ×*g* for 1 min, resuspended by gentle pipetting, and cooled down on ice followed by sorting of VF405$^+$GFP$^+$ or VF405$^+$ cells at 4–5°C. For Myc-CD80 cis depletion in Jurkat cells coexpressing Myc-CD80 and CTLA4-GFP in Fig. 7 D, Jurkat cells were stimulated by 10 µg/ml plate-bound Okt3 (#317326; BioLegend) rather than by Raji cells. After stimulation, T cells were incubated in complete RPMI medium containing no blocking agents, 100 µg/ml ipilimumab, 20 µg/ml MBP-28.3scFv, or 100 µg/ml ipilimumab and 20 µg/ml MBP-28.3scFv combined for 30 min at 4°C before mixing with 30-fold excess of *CD28*$^{-/-}$ Jurkat filler cells or the same volume of RPMI; cell mixtures were seeded at 2 million/well in a flat-bottom 24-well plate or 0.18 million/well in a 96-well plate, and then centrifuged at 300 ×*g* for 1 min to form a monolayer. After further incubation at 37°C or on ice for indicated hours, cells were fixed and stained with anti-CD80, anti-CD86, or anti–HLA-DR antibodies before flow cytometry analysis. For anti-Myc staining, cells were stained without fixation at indicated time points and subjected to flow cytometry analysis.

CD4$^+$ T cells autostimulation and DC:CD4$^+$ T cells coculture assays

For Fig. 4, VF405-stained CD4$^+$ T cells were preincubated with indicated Raji APCs for 15 min and sorted for VF405$^+$ or VF405$^+$GFP$^+$ population. This short incubation was sufficient for trogocytosis of B7 and MHC but not long enough to induce endogenous B7 expression in T cells. For DC coculture, 0.1 million sorted T cells were cultured with mature DCs derived from human monocytes of a different donor in the presence of SEB at a ratio (DC:T) of 1:10 or 1:30 for indicated time. DC maturation was induced as previously described (Zhao et al., 2019). Brefeldin A (#420601; BioLegend) was added 6 h prior to the fixation and permeabilization of cells using Cyto-Fast Fix/Perm Buffer Set (#426803; BioLegend), followed by intracellular staining of anti-human IL-2 (#503814; BioLegend) and anti-human IFNγ (#502539; BioLegend). For autostimulation assay, T cells were incubated in complete RPMI medium containing 100 ng/ml SEB with or without 100 µg/ml ipilimumab for 30 min at 4°C, followed by a further incubation at 37°C for indicated time periods. Culture medium was renewed every 24 h with medium containing no blocking agents or 100 µg/ml ipilimumab. Supernatants at 24, 48, 72, and 96 h were harvested, diluted, and measured using IL-2 ELISA kit (#431804; BioLegend).

Jurkat cell–intrinsic depletion assay followed by confocal microscopy

Raji cells and 10 million of the VF405-stained Jurkat cells were mixed and centrifuged at 300 ×*g* for 1 min to initiate cell:cell contact, after which the cocultures were immediately transferred to a 37°C water bath and incubated for 15 min. Cocultures were resuspended in ice-cold complete RPMI medium, then VF405$^+$GFP$^+$ Jurkat cells were sorted, centrifuged to the bottom of a flat-bottom 24-well plate, and incubated at a density of 20,000 cells/well in complete RPMI medium containing no blocking agents or 100 µg/ml ipilimumab for 30 min at 4°C before a further incubation ranging from 0 to 120 min at 37°C, and these cells were fixed with 2% PFA for 15 min at room temperature and observed using confocal microscopy. 0.1 million fixed cells were loaded into a 96-well glass-bottom plate for confocal microscopy assays. Images were acquired with a Nikon spinning-disk confocal microscope, then processed and quantified using Fiji. To quantify the fluorescence intensities (FI) of CD80 that colocalized with CD28 or CTLA4, mask images identifying the area of CD80 were generated by applying the "subtract background" command to CD80 (GFP) images using the default setting (Xu et al., 2021). Because the majority of CD80 signals colocalized with both CD28 and CTLA4 to some degree, the CD28 FI (JF646) and CTLA4 FI (mCherry) in the mask-

overlaid images were measured and used to calculate the relative CD80 FI on CTLA4 using the equation: CD80 FI on CTLA4 = total CD80 FI × masked CTLA4 FI/(masked CD28 FI + masked CTLA4 FI) for each cell. Representative images from n = 40 isolated single T cells were quantified for each sample.

B7-Ig staining of Jurkat cells expressing CTLA4$^{\Delta ICD}$ alone or coexpressing CTLA4$^{\Delta ICD}$ and B7

CD28$^{-/-}$*CTLA4*$^{\Delta ICD}$*-mCherry*$^{+}$, *CD28*$^{-/-}$*CTLA4*$^{\Delta ICD}$*-mCherry*$^{+}$*CD80*$^{+}$, or *CD28*$^{-/-}$*CTLA4*$^{\Delta ICD}$*-mCherry*$^{+}$*CD86*$^{+}$ Jurkat cells were incubated with 10 µg/ml soluble CD80-Ig (#10698-H02H-100; Sino Biological) or CD86-Ig (#775606; BioLegend) on ice for 30 min, washed twice with 1× PBS containing 2% FBS, and then incubated with 3 µg/ml Alexa Fluor 647 anti-human IgFc (#409320; BioLegend) on ice for 30 min, followed by fixation with 2% PFA at room temperature for 15 min. Cells were subjected to either imaging on a Nikon Ti2 spinning-disk confocal microscope or flow cytometry analysis. Confocal images were then processed and the FI of Alexa Fluor 647 was quantified using Fiji.

Flow cytometry

Flow cytometry was conducted using an LSRFortessa cell analyzer (BD Biosciences). Indicated Treg, Tconv, Jurkat cells, Raji cells, or indicated cocultures were resuspended with ice-cold FACS buffer (PBS 2% FBS) and analyzed immediately, or after fixation and staining with indicated antibodies. For cell permeabilization, cells were fixed with 2% PFA for 15 min at room temperature, permeabilized with 0.1% Saponin in FACS buffer, and then stained in 0.02% Saponin containing FACS buffer. For FoxP3 staining, True-Nuclear Transcription Factor Buffer Set (#424401; BioLegend) was used to fix and permeabilize the cells according to the manufacturer instructions before staining with Brilliant Violet 421 anti-FoxP3 antibody (#320123; BioLegend). Flow cytometry data were analyzed using FlowJo (FlowJo, LLC).

Quantification and statistical analysis

All data with replicates were shown as mean ± SD, and number of replicates is indicated in figure legends. Curve fitting and normalization were performed in GraphPad Prism 8 (GraphPad). Statistical significance was evaluated by unpaired two-tailed Student's *t* test (*, P < 0.05; **, P < 0.01; ***, P < 0.001; ****, P < 0.0001). Data with P < 0.05 are considered statistically significant.

Online supplemental material

Fig. S1 shows gating strategy and protein expression levels related to Fig. 2. Fig. S2 shows that CTLA4 partially contributed to the acquisition of B7 in Jurkat (CD28$^{+/+}$CTLA4^{high}) cells, related to Fig. 3. Fig. S3 shows gating strategy and DC profiling for cell culture assays, related to Fig. 4. Fig. S4 presents confocal microscopy images showing filler cell inhibition of T–T contacts. Fig. S5 shows that CTLA4-mediated CD80 cis depletion is promoted by TCR stimulation.

Data availability

All data associated with this study are presented in the article or supplemental materials. Further information and requests for new reagents generated in this study may be directed to and will be fulfilled by the lead contact, Enfu Hui.

Acknowledgments

We thank E. Griffis (Nikon Imaging Center of University of California, San Diego) for help with imaging, Luke Lavis (Janelia Research Campus, Ashburn, VA, USA) for providing HaloTag ligands, Sam Sherrard-Kefford for providing some illustrations, and Isaac Chang for critical review of the manuscript.

This work was supported by R37 CA239072 (to E. Hui) and R01 AG074273 (to X. Chen) from the National Institute of Health, a Searle Scholar Award (to E. Hui) from the Kinship Foundation, a Pew Biomedical Scholar Award (to E. Hui) from the Pew Charitable Trusts, and the Hartwell Foundation grant to J. Bui. Y. Zhao was supported by the Irvington postdoctoral fellowship from the Cancer Research Institute.

Author contributions: Methodology: X. Xu, P. Dennett, J. Zhang, Y. Zhao, T. Masubuchi, and A. Sherrard. Investigation: X. Xu, P. Dennett, and J. Zhang. Visualization: X. Xu, P. Dennett, J. Zhang, and A. Sherrard. Funding acquisition: X. Chen and E. Hui. Project administration: E. Hui. Supervision: J. Bui, X. Chen, and E. Hui. Writing—original draft: P. Dennett, X. Xu, J. Zhang, and E. Hui. Writing—review & editing: P. Dennett, X. Xu, J. Zhang, and E. Hui.

Disclosures: The authors declare no competing interests exist.

Submitted: 14 August 2022
Revised: 16 February 2023
Accepted: 16 March 2023

References

Akkaya, B., Y. Oya, M. Akkaya, J. Al Souz, A.H. Holstein, O. Kamenyeva, J. Kabat, R. Matsumura, D.W. Dorward, D.D. Glass, and E.M. Shevach. 2019. Regulatory T cells mediate specific suppression by depleting peptide-MHC class II from dendritic cells. *Nat. Immunol.* 20:218–231. https://doi.org/10.1038/s41590-018-0280-2

Akkaya, B., and E.M. Shevach. 2020. Regulatory T cells: Master thieves of the immune system. *Cell. Immunol.* 355:104160. https://doi.org/10.1016/j.cellimm.2020.104160

Al-Yassin, G.A., and P.A. Bretscher. 2018. Does T cell activation require a quorum of lymphocytes? *J. Immunol.* 201:2855–2861. https://doi.org/10.4049/jimmunol.1800805

Attanasio, J., and E.J. Wherry. 2016. Costimulatory and coinhibitory receptor pathways in infectious disease. *Immunity*. 44:1052–1068. https://doi.org/10.1016/j.immuni.2016.04.022

Azuma, M., H. Yssel, J.H. Phillips, H. Spits, and L.L. Lanier. 1993. Functional expression of B7/BB1 on activated T lymphocytes. *J. Exp. Med.* 177:845–850. https://doi.org/10.1084/jem.177.3.845

Bachmann, M.F., G. Köhler, B. Ecabert, T.W. Mak, and M. Kopf. 1999. Cutting edge: Lymphoproliferative disease in the absence of CTLA-4 is not T cell autonomous. *J. Immunol.* 163:1128–1131. https://doi.org/10.4049/jimmunol.163.3.1128

Boccasavia, V.L., E.R. Bovolenta, A. Villanueva, A. Borroto, C.L. Oeste, H.M. van Santen, C. Prieto, D. Alonso-López, M.D. Diaz-Muñoz, F.D. Batista, and B. Alarcón. 2021. Antigen presentation between T cells drives Th17 polarization under conditions of limiting antigen. *Cell Rep.* 34:108861. https://doi.org/10.1016/j.celrep.2021.108861

Bretscher, P.A. 2014a. The activation and inactivation of mature CD4 T cells: A case for peripheral self-nonself discrimination. *Scand. J. Immunol.* 79:348–360. https://doi.org/10.1111/sji.12173

Bretscher, P.A. 2014b. On the mechanism determining the TH1/TH2 phenotype of an immune response, and its pertinence to strategies for the prevention, and treatment, of certain infectious diseases. *Scand. J. Immunol.* 79:361–376. https://doi.org/10.1111/sji.12175

Butler, T.C., M. Kardar, and A.K. Chakraborty. 2013. Quorum sensing allows T cells to discriminate between self and nonself. *Proc. Natl. Acad. Sci. USA.* 110:11833–11838. https://doi.org/10.1073/pnas.1222467110

Davis, D.M. 2007. Intercellular transfer of cell-surface proteins is common and can affect many stages of an immune response. *Nat. Rev. Immunol.* 7:238–243. https://doi.org/10.1038/nri2020

Egen, J.G., and J.P. Allison. 2002. Cytotoxic T lymphocyte antigen-4 accumulation in the immunological synapse is regulated by TCR signal strength. *Immunity*. 16:23–35. https://doi.org/10.1016/S1074-7613(01)00259-X

Gérard, A., O. Khan, P. Beemiller, E. Oswald, J. Hu, M. Matloubian, and M.F. Krummel. 2013. Secondary T cell-T cell synaptic interactions drive the differentiation of protective CD8+ T cells. *Nat. Immunol.* 14:356–363. https://doi.org/10.1038/ni.2547

Greenwald, R.J., V.A. Boussiotis, R.B. Lorsbach, A.K. Abbas, and A.H. Sharpe. 2001. CTLA-4 regulates induction of anergy in vivo. *Immunity*. 14:145–155. https://doi.org/10.1016/S1074-7613(01)00097-8

He, M., Y. Chai, J. Qi, C.W.H. Zhang, Z. Tong, Y. Shi, J. Yan, S. Tan, and G.F. Gao. 2017. Remarkably similar CTLA-4 binding properties of therapeutic ipilimumab and tremelimumab antibodies. *Oncotarget*. 8:67129–67139. https://doi.org/10.18632/oncotarget.18004

Helft, J., A. Jacquet, N.T. Joncker, I. Grandjean, G. Dorothée, A. Kissenpfennig, B. Malissen, P. Matzinger, and O. Lantz. 2008. Antigen-specific T-T interactions regulate CD4 T-cell expansion. *Blood*. 112:1249–1258. https://doi.org/10.1182/blood-2007-09-114389

Holling, T.M., E. Schooten, and P.J. van Den Elsen. 2004. Function and regulation of MHC class II molecules in T-lymphocytes: Of mice and men. *Hum. Immunol.* 65:282–290. https://doi.org/10.1016/j.humimm.2004.01.005

Hou, T.Z., O.S. Qureshi, C.J. Wang, J. Baker, S.P. Young, L.S. Walker, and D.M. Sansom. 2015. A transendocytosis model of CTLA-4 function predicts its suppressive behavior on regulatory T cells. *J. Immunol.* 194:2148–2159. https://doi.org/10.4049/jimmunol.1401876

Hwang, I., J.F. Huang, H. Kishimoto, A. Brunmark, P.A. Peterson, M.R. Jackson, C.D. Surh, Z. Cai, and J. Sprent. 2000. T cells can use either T cell receptor or CD28 receptors to absorb and internalize cell surface molecules derived from antigen-presenting cells. *J. Exp. Med.* 191:1137–1148. https://doi.org/10.1084/jem.191.7.1137

Joly, E., and D. Hudrisier. 2003. What is trogocytosis and what is its purpose?. *Nat. Immunol.* 4:815. https://doi.org/10.1038/ni0903-815

Kremer, J.M., R. Westhovens, M. Leon, E. Di Giorgio, R. Alten, S. Steinfeld, A. Russell, M. Dougados, P. Emery, I.F. Nuamah, et al. 2003. Treatment of rheumatoid arthritis by selective inhibition of T-cell activation with fusion protein CTLA4Ig. *N. Engl. J. Med.* 349:1907–1915. https://doi.org/10.1056/NEJMoa035075

Kuehn, H.S., W. Ouyang, B. Lo, E.K. Deenick, J.E. Niemela, D.T. Avery, J.N. Schickel, D.Q. Tran, J. Stoddard, Y. Zhang, et al. 2014. Immune dysregulation in human subjects with heterozygous germline mutations in CTLA4. *Science*. 345:1623–1627. https://doi.org/10.1126/science.1255904

Leach, D.R., M.F. Krummel, and J.P. Allison. 1996. Enhancement of antitumor immunity by CTLA-4 blockade. *Science*. 271:1734–1736. https://doi.org/10.1126/science.271.5256.1734

Leung, H.T., J. Bradshaw, J.S. Cleaveland, and P.S. Linsley. 1995. Cytotoxic T lymphocyte-associated molecule-4, a high-avidity receptor for CD80 and CD86, contains an intracellular localization motif in its cytoplasmic tail. *J. Biol. Chem.* 270:25107–25114. https://doi.org/10.1074/jbc.270.42.25107

Linsley, P.S., J. Bradshaw, J. Greene, R. Peach, K.L. Bennett, and R.S. Mittler. 1996. Intracellular trafficking of CTLA-4 and focal localization towards sites of TCR engagement. *Immunity*. 4:535–543. https://doi.org/10.1016/S1074-7613(00)80480-X

Maranto, A.R. 1982. Neuronal mapping: A photooxidation reaction makes lucifer yellow useful for electron microscopy. *Science*. 217:953–955. https://doi.org/10.1126/science.7112109

Metz, D.P., D.L. Farber, T. Taylor, and K. Bottomly. 1998. Differential role of CTLA-4 in regulation of resting memory versus naive CD4 T cell activation. *J. Immunol.* 161:5855–5861. https://doi.org/10.4049/jimmunol.161.11.5855

Miyake, K., and H. Karasuyama. 2021. The role of trogocytosis in the modulation of immune cell functions. *Cells*. 10:1255. https://doi.org/10.3390/cells10051255

Nakada-Tsukui, K., and T. Nozaki. 2021. Trogocytosis in Unicellular Eukaryotes. *Cells*. 10:2975. https://doi.org/10.3390/cells10112975

Parks, A.L., K.M.Klueg, J.R.Stout, andM.A.Muskavitch. 2000. Ligand endocytosis drives receptor dissociation and activation in the Notch pathway. *Development*. 127:1373–1385. https://doi.org/10.1242/dev.127.7.1373

Patel, D.M., R.W. Dudek, and M.D. Mannie. 2001. Intercellular exchange of class II MHC complexes: Ultrastructural localization and functional presentation of adsorbed I-A/peptide complexes. *Cell. Immunol.* 214:21–34. https://doi.org/10.1006/cimm.2002.1887

Qureshi, O.S., Y. Zheng, K. Nakamura, K. Attridge, C. Manzotti, E.M. Schmidt, J. Baker, L.E. Jeffery, S. Kaur, Z. Briggs, et al. 2011. Trans-endocytosis of CD80 and CD86: A molecular basis for the cell-extrinsic function of CTLA-4. *Science*. 332:600–603. https://doi.org/10.1126/science.1202947

Ribas, A., and J.D. Wolchok. 2018. Cancer immunotherapy using checkpoint blockade. *Science*. 359:1350–1355. https://doi.org/10.1126/science.aar4060

Rudulier, C.D., K.K. McKinstry, G.A. Al-Yassin, D.R. Kroeger, and P.A. Bretscher. 2014. The number of responding CD4 T cells and the dose of antigen conjointly determine the TH1/TH2 phenotype by modulating B7/CD28 interactions. *J. Immunol.* 192:5140–5150. https://doi.org/10.4049/jimmunol.1301691

Sabzevari, H., J. Kantor, A. Jaigirdar, Y. Tagaya, M. Naramura, J. Hodge, J. Bernon, and J. Schlom. 2001. Acquisition of CD80 (B7-1) by T cells. *J. Immunol.* 166:2505–2513. https://doi.org/10.4049/jimmunol.166.4.2505

Salomon, B., and J.A. Bluestone. 2001. Complexities of CD28/B7: CTLA-4 costimulatory pathways in autoimmunity and transplantation. *Annu. Rev. Immunol.* 19:225–252. https://doi.org/10.1146/annurev.immunol.19.1.225

Schildberg, F.A., S.R. Klein, G.J. Freeman, and A.H. Sharpe. 2016. Coinhibitory pathways in the B7-CD28 ligand-receptor family. *Immunity*. 44:955–972. https://doi.org/10.1016/j.immuni.2016.05.002

Schindelin, J., I. Arganda-Carreras, E. Frise, V. Kaynig, M. Longair, T. Pietzsch, S. Preibisch, C. Rueden, S. Saalfeld, B. Schmid, et al. 2012. Fiji: An open-source platform for biological-image analysis. *Nat. Methods*. 9:676–682. https://doi.org/10.1038/nmeth.2019

Schneider, H., J. Downey, A. Smith, B.H. Zinselmeyer, C. Rush, J.M. Brewer, B. Wei, N. Hogg, P. Garside, and C.E. Rudd. 2006. Reversal of the TCR stop signal by CTLA-4. *Science*. 313:1972–1975. https://doi.org/10.1126/science.1131078

Schriek, P., A.C. Ching, N.S. Moily, J. Moffat, L. Beattie, T.M. Steiner, L.M. Hosking, J.M. Thurman, V.M. Holers, S. Ishido, et al. 2022. Marginal zone B cells acquire dendritic cell functions by trogocytosis. *Science*. 375:eabf7470. https://doi.org/10.1126/science.abf7470

Tai, X., F. Van Laethem, L. Pobezinsky, T. Guinter, S.O. Sharrow, A. Adams, L. Granger, M. Kruhlak, T. Lindsten, C.B. Thompson, et al. 2012. Basis of CTLA-4 function in regulatory and conventional CD4(+) T cells. *Blood*. 119:5155–5163. https://doi.org/10.1182/blood-2011-11-388918

Tai, X., F. Van Laethem, A.H. Sharpe, and A. Singer. 2007. Induction of autoimmune disease in CTLA-4-/- mice depends on a specific CD28 motif that is required for in vivo costimulation. *Proc. Natl. Acad. Sci. USA.* 104:13756–13761. https://doi.org/10.1073/pnas.0706509104

Tatari-Calderone, Z., R.T. Semnani, T.B. Nutman, J. Schlom, and H. Sabzevari. 2002. Acquisition of CD80 by human T cells at early stages of activation: Functional involvement of CD80 acquisition in T cell to T cell interaction. *J. Immunol.* 169:6162–6169. https://doi.org/10.4049/jimmunol.169.11.6162

Teft, W.A., M.G. Kirchhof, and J. Madrenas. 2006. A molecular perspective of CTLA-4 function. *Annu. Rev. Immunol.* 24:65–97. https://doi.org/10.1146/annurev.immunol.24.021605.090535

Tekguc, M., J.B. Wing, M. Osaki, J. Long, and S. Sakaguchi. 2021. Treg-expressed CTLA-4 depletes CD80/CD86 by trogocytosis, releasing free PD-L1 on antigen-presenting cells. *Proc. Natl. Acad. Sci. USA.* 118:e2023739118. https://doi.org/10.1073/pnas.2023739118

Trzupek, D., M. Dunstan, A.J. Cutler, M. Lee, L. Godfrey, L. Jarvis, D.B. Rainbow, D. Aschenbrenner, J.L. Jones, and H.H. Uhlig. 2020. Discovery of CD80 and CD86 as recent activation markers on regulatory T cells by protein-RNA single-cell analysis. *Genome Med.* 12:55. https://doi.org/10.1186/s13073-020-00756-z

Valk, E., C.E. Rudd, and H. Schneider. 2008. CTLA-4 trafficking and surface expression. *Trends Immunol.* 29:272–279. https://doi.org/10.1016/j.it.2008.02.011

Vanhove, B., G. Laflamme, F. Coulon, M. Mougin, P. Vusio, F. Haspot, J. Tiollier, and J.P. Soulillou. 2003. Selective blockade of CD28 and not

CTLA-4 with a single-chain Fv-alpha1-antitrypsin fusion antibody. *Blood*. 102:564–570. https://doi.org/10.1182/blood-2002-08-2480

Walker, L.S., and D.M. Sansom. 2011. The emerging role of CTLA4 as a cell-extrinsic regulator of T cell responses. *Nat. Rev. Immunol.* 11:852–863. https://doi.org/10.1038/nri3108

Walker, L.S., and D.M. Sansom. 2015. Confusing signals: Recent progress in CTLA-4 biology. *Trends Immunol.* 36:63–70. https://doi.org/10.1016/j.it.2014.12.001

Watanabe, M., S. Celli, F.A. Alkhaleel, and R.J. Hodes. 2022. Antigen-presenting T cells provide critical B7 co-stimulation for thymic iNKT cell development via CD28-dependent trogocytosis. *Cell Rep.* 41:111731. https://doi.org/10.1016/j.celrep.2022.111731

Wei, S.C., C.R. Duffy, and J.P. Allison. 2018. Fundamental mechanisms of immune checkpoint blockade therapy. *Cancer Discov.* 8:1069–1086. https://doi.org/10.1158/2159-8290.CD-18-0367

Wei, S.C., R. Sharma, N.A.S. Anang, J.H. Levine, Y. Zhao, J.J. Mancuso, M. Setty, P. Sharma, J. Wang, D. Pe'er, and J.P. Allison. 2019. Negative Co-stimulation constrains T cell differentiation by imposing boundaries on possible cell States. *Immunity*. 50:1084–1098.e10. https://doi.org/10.1016/j.immuni.2019.03.004

Wertheimer, T., M. Dohse, G. Afram, D. Weber, M. Heidenreich, B. Holler, A.S. Kattner, A. Neubauer, S. Mielke, P. Ljungman, et al. 2021. Abatacept as salvage therapy in chronic graft-versus-host disease-a retrospective analysis. *Ann. Hematol.* 100:779–787. https://doi.org/10.1007/s00277-021-04434-x

Wing, K., Y. Onishi, P. Prieto-Martin, T. Yamaguchi, M. Miyara, Z. Fehervari, T. Nomura, and S. Sakaguchi. 2008. CTLA-4 control over Foxp3+ regulatory T cell function. *Science*. 322:271–275. https://doi.org/10.1126/science.1160062

Wing, K., T. Yamaguchi, and S. Sakaguchi. 2011. Cell-autonomous and -non-autonomous roles of CTLA-4 in immune regulation. *Trends Immunol.* 32:428–433. https://doi.org/10.1016/j.it.2011.06.002

Xiang, J., H. Huang, and Y. Liu. 2005. A new dynamic model of CD8+ T effector cell responses via CD4+ T helper-antigen-presenting cells. *J. Immunol.* 174:7497–7505. https://doi.org/10.4049/jimmunol.174.12.7497

Xu, X., T. Masubuchi, Q. Cai, Y. Zhao, and E. Hui. 2021. Molecular features underlying differential SHP1/SHP2 binding of immune checkpoint receptors. *eLife*. https://doi.org/10.7554/eLife.74276

Xu, X., B. Hou, A. Fulzele, T. Masubuchi, Y. Zhao, Z. Wu, Y. Hu, Y. Jiang, Y. Ma, H. Wang, et al. 2020. PD-1 and BTLA regulate T cell signaling differentially and only partially through SHP1 and SHP2. *J Cell Biol.* 219:e201905085. https://doi.org/10.1083/jcb.201905085

ZakeriB., J.O.Fierer, E.Celik, E.C.Chittock, U. Schwarz-Linek, V.T. Moy, andM.Howarth. 2012. Peptide tag forming a rapid covalent bond to a protein, through engineering a bacterial adhesin. *Proc. Natl. Acad. Sci. USA*. 109:E690–E697. https://doi.org/10.1073/pnas.1115485109

Zenke, S., M.M. Palm, J. Braun, A. Gavrilov, P. Meiser, J.P. Böttcher, N. Beyersdorf, S. Ehl, A. Gerard, T. Lämmermann, et al. 2020. Quorum regulation via nested antagonistic feedback circuits mediated by the receptors CD28 and CTLA-4 confers robustness to T cell population dynamics. *Immunity*. 52:313–327.e7. https://doi.org/10.1016/j.immuni.2020.01.018

Zenke, S., M.P. Sica, F. Steinberg, J. Braun, A. Zink, A. Gavrilov, A. Hilger, A. Arra, M. Brunner-Weinzierl, R. Elling, et al. 2022. Differential trafficking of ligands trogocytosed via CD28 versus CTLA4 promotes collective cellular control of co-stimulation. *Nat. Commun.* 13:6459. https://doi.org/10.1038/s41467-022-34156-1

Zhao, Y., C.K. Lee, C.H. Lin, R.B. Gassen, X. Xu, Z. Huang, C. Xiao, C. Bonorino, L.F. Lu, J.D. Bui, and E. Hui. 2019. PD-L1:CD80 Cis-Heterodimer triggers the Co-stimulatory receptor CD28 while repressing the inhibitory PD-1 and CTLA-4 pathways. *Immunity*. 51:1059–1073.e9. https://doi.org/10.1016/j.immuni.2019.11.003

Zhao, Y., C. Caron, Y.-Y. Chan, C.K. Lee, X. Xu, J. Zhang, T. Masubuchi, C. Wu, J.D. Bui, and X. Hui. 2023. Cis-B7:CD28 Interactions at Invaginated Synaptic Membranes Activate CD28 and Promote CD8+ T Cell Function and Anti-Tumor Immunity. *Immunity*. In press.

Supplemental material

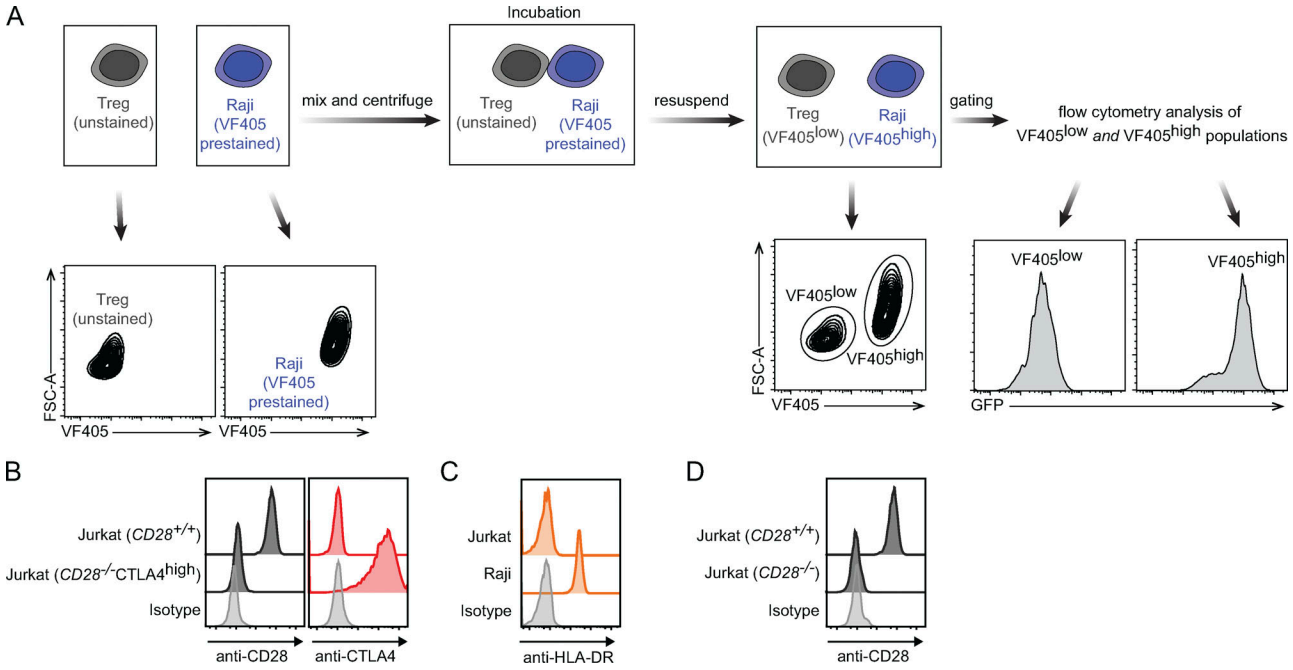

Figure S1. **Gating strategy and protein expression levels related to** Fig. 2**. (A)** Upper: Experimental scheme depicting the method of gating Tregs or Raji cells in coculture. Lower: Flow cytometry contour maps or histograms before and after mixing of Tregs and VF-405 prestained Raji cells. **(B)** Flow cytometry histograms showing the CD28 and CTLA4 total levels on Jurkat (*CD28*$^{+/+}$) and Jurkat (*CD28*$^{-/-}$CTLA4^{high}) cells. **(C)** Flow cytometry histograms showing the MHC II (anti–HLA-DR) levels on Jurkat and Raji cells. **(D)** Flow cytometry histograms showing the CD28 levels on Jurkat (*CD28*$^{+/+}$) and Jurkat (*CD28*$^{-/-}$) cells.

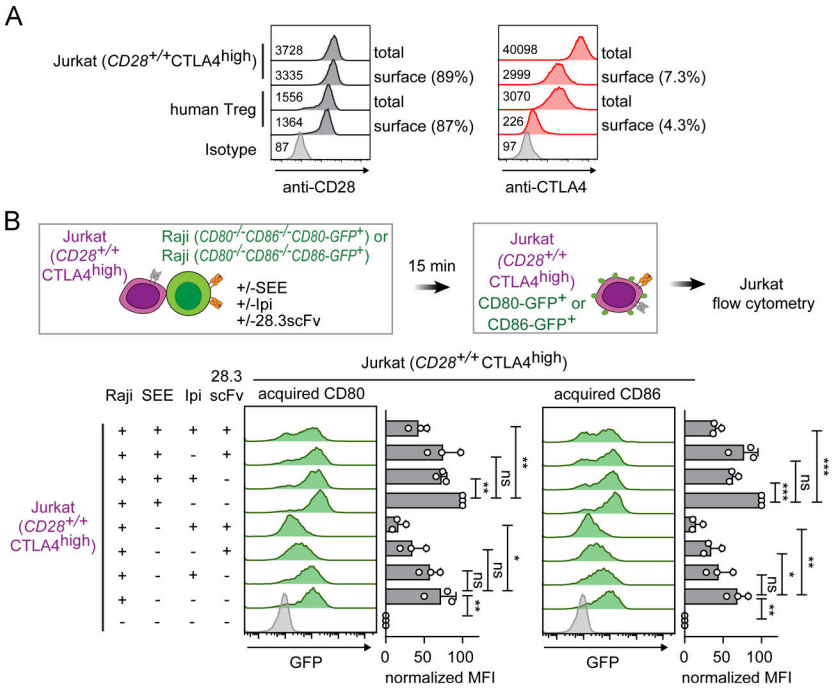

Figure S2. **CTLA4 partially contributed to the acquisition of B7 in Jurkat (*CD28*$^{+/+}$CTLA4^{high}) cells, related to** Fig. 3. **(A)** FACS histograms showing the total and surface levels of CD28 and CTLA4 on Tregs and Jurkat (*CD28*$^{+/+}$CTLA4^{high}) cells, numbers on the left of histograms showing the MFI values. **(B)** Effects of CTLA4 and/or CD28 blockade on the abilities of Jurkat to acquire CD80 and CD86. Upper: Schematics of a Jurkat:Raji coculture assay examining Jurkat-mediated acquisition of B7 ligands from APCs. Lower: Representative FACS histograms showing the CD80-GFP or CD86-GFP levels on Jurkat (*CD28*$^{+/+}$CTLA4^{high}) cells after a 15-min incubation with either *CD80*$^{-/-}$*CD86*$^{-/-}$*CD80-GFP*$^{+}$ or *CD80*$^{-/-}$*CD86*$^{-/-}$*CD86-GFP*$^{+}$ Raji cells. Bar graphs on the immediate right show the normalized MFI values of acquired CD80-GFP or CD86-GFP on Jurkat cells, calculated by setting the MFI of "–, –, –, –" condition as 0 and the MFI of "+, +, –, –" condition as 100. Error bars are SD from three independent coculture experiments performed on three different days. *, P < 0.05; **, P < 0.01; ***, P < 0.001; unpaired two-tailed Student's *t* test.

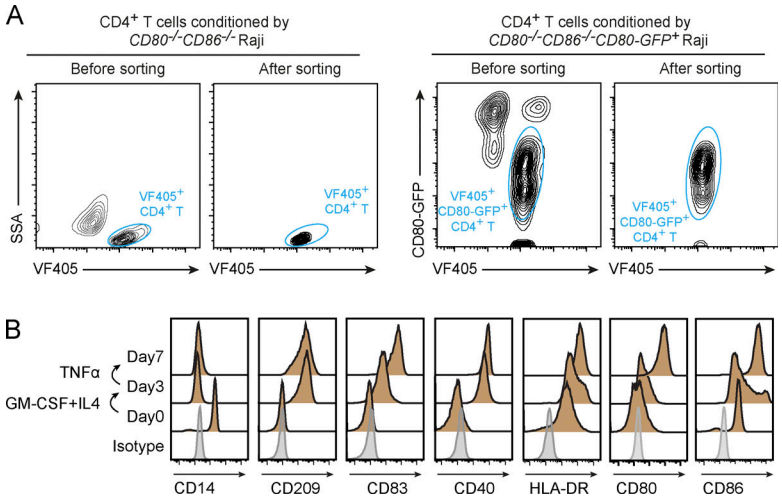

Figure S3. **Gating strategy and DC profiling for cell culture assays, related to** Fig. 4. **(A)** Gating strategy of human CD4^{+} T cells preconditioned with indicated Raji APCs. **(B)** FACS histograms showing the expression of indicated cell surface markers during DC maturation from human monocytes.

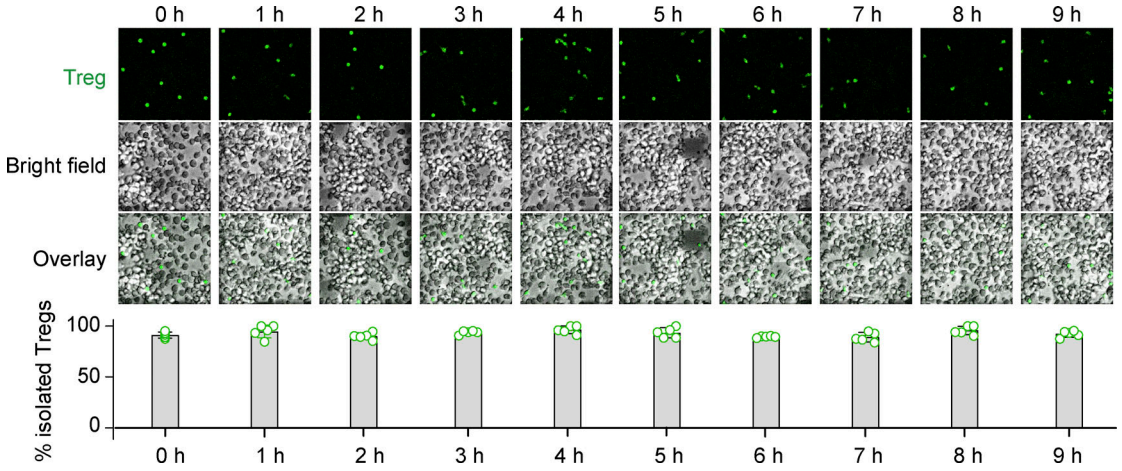

Figure S4. **Confocal microscopy images showing filler cells inhibition of T–T contacts.** Treg cells were prestained with VF405 dye (rendered as green) and mixed with 30-fold excess unstained filler cells (shown as gray) before centrifugation onto a flat-bottom plate to form monolayer followed by incubation at 37°C. Shown are representative confocal images of the indicated channels of a randomly selected field taken at indicated time points. Bar graph summarizes the percentage of isolated Treg cells from five different image fields, calculated as (the number of Treg cells not in physical contact with another Treg cell)/(the total number of Treg cells) × 100. Each data point in the bar graph corresponds to the percentage of isolated Treg cells in a randomly selected image field.

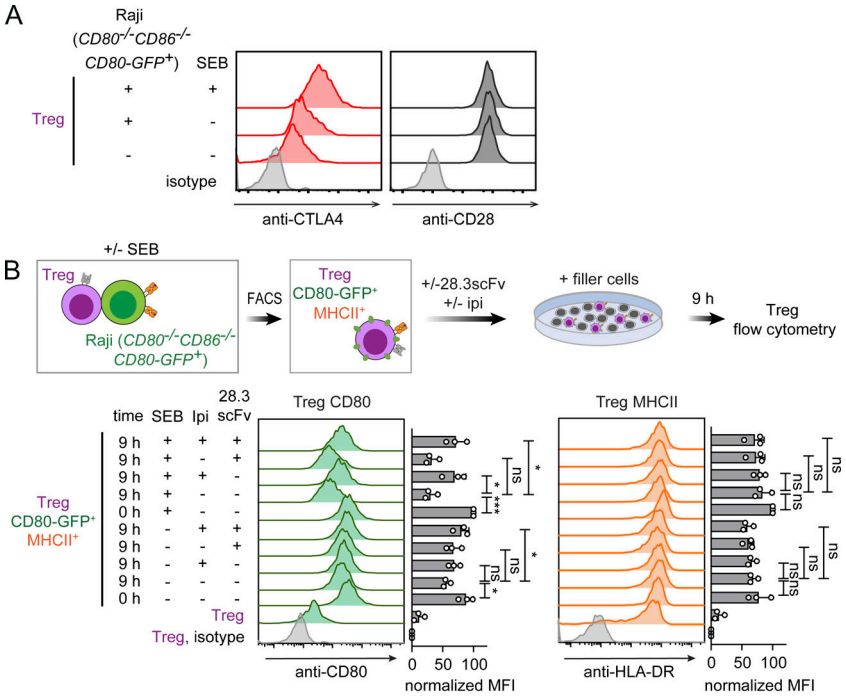

Figure S5. **CTLA4-mediated CD80 cis depletion is promoted by TCR stimulation. (A)** FACS histograms showing surface levels of CTLA4 and CD28 on human Tregs after 12 h coculture with Raji (*CD80*$^{-/-}$*CD86*$^{-/-}$*CD80-GFP*$^{+}$) in the presence or absence of SEB. **(B)** Upper: Experimental scheme. Human Tregs were precultured with CD80-GFP-expressing Raji (*CD80-GFP*$^{+}$*CD80*$^{-/-}$*CD86*$^{-/-}$) in the presence or absence of SEB, isolated by FACS, and incubated with 30-fold excess of *CD28*$^{-/-}$ Jurkat filler cells for 9 h, in the presence or absence of ipilimumab and/or 28.3scFv before FACS measurement of CD80 and HLA-DR amounts. Lower: Representative FACS histograms and quantification graph of CD80 and HLA-DR amounts on Tregs before (0 h) and after 9 h incubation under the indicated conditions. Tregs at 0 h were preconditioned by Raji (*CD80*$^{-/-}$*CD86*$^{-/-}$*CD80-GFP*$^{+}$) as shown in A. Normalized MFIs of anti-CD80 and anti–HLA-DR were calculated by setting the MFI of "Treg, isotype" as 0 and the MFI of "0 h, +, –, –" as 100. Error bars are SD from three independent coculture experiments, data were generated using PBMCs from three independent age-matched donors. *, P < 0.05; ***, P < 0.001; unpaired two-tailed Student's *t* test.